bioRxiv preprint doi: https://doi.org/10.1101/2021.05.07.443077; this version posted May 8, 2021. The copyright holder for this preprint (which was not certified by peer review) is the author/funder, who has granted bioRxiv a license to display the preprint in perpetuity. It is made available under aCC-BY 4.0 International license.

Full title: Analysis of melanotic *Plasmodium* spp. capsules in mosquitoes reveal eumelanin-pheomelanin composition and identify *Ag*Mesh as a modulator of parasite infection.

Short title: Dissection of mosquito melanotic capsules.

Emma Camacho[1], Yuemei Dong[1], Yesseinia Anglero-Rodriguez[1], Daniel Smith[1], Ricardo de Souza Jacomini[2,3], George Dimopoulos[1] and Arturo Casadevall[1*]

[1] W. Harry Feinstone Department of Molecular Microbiology and Immunology, Bloomberg School of Public Health, Johns Hopkins University, Baltimore, Maryland, United States of America.

[2] Department of Neurology, School of Medicine, Johns Hopkins University, Baltimore, Maryland, United States of America.

[3] Lieber Institute for Brain Development, Johns Hopkins University, Baltimore, Maryland, United States of America.

* Corresponding author

E-mail: acasade1@jhu.edu

bioRxiv preprint doi: https://doi.org/10.1101/2021.05.07.443077; this version posted May 8, 2021. The copyright holder for this preprint (which was not certified by peer review) is the author/funder, who has granted bioRxiv a license to display the preprint in perpetuity. It is made available under aCC-BY 4.0 International license.

ABSTRACT

Melanins are structurally complex pigments produced by organisms in all domains of life from bacteria to animals, including humans. In insects, melanins are essential for survival and have key roles in cuticle sclerotization, wound healing and innate immunity. In this study, we used a diverse set of molecular, biochemical, and imaging approaches to characterize mosquito melanin involved in innate immune defense (melanotic capsules). We observed that melanotic capsules enclosing *Plasmodium berghei* ookinetes were composed of an acid-resistant and highly hydrophobic material with granular appearance, which are characteristic properties of melanins. Spectroscopical analyses reveal chemical signatures of eumelanins and pheomelanin. Furthermore, using an enrichment approach for the proteomic analysis, we identified a set of 14 of acid-resistant mosquito proteins embedded within the melanin matrix possibly related to an anti-*Plasmodium* response. Among these, *Ag*Mesh, a highly conserved protein among insect species that contains domains suggesting a role in immune recognition and function. We targeted *Ag*Mesh for further study using a RNAi-based gene silencing approach in mosquitos and challenged them with two *Plasmodium* spp. Surprisingly, *Ag*Mesh gene silencing in mosquitos was associated with reduced parasite infection, implying an important role in facilitating vector infection by *Plasmodium* spp. Our results provide a new approach to study aspects of insect melanogenesis that revealed proteins associated with melanotic capsule, one of which was strongly implicated in the pathogenesis of *Plasmodium* spp. mosquito infection. Given the conservation of *Ag*Mesh among disease-transmitting insect vector species, future analysis of this protein could provide fertile ground for the identification of strategies that block transmission of disease to humans.

Keywords: Malaria, *Anopheles*, *Plasmodium*, Innate immune response, Melanization, Melanin, Eumelanin, Pheomelanin

bioRxiv preprint doi: https://doi.org/10.1101/2021.05.07.443077; this version posted May 8, 2021. The copyright holder for this preprint (which was not certified by peer review) is the author/funder, who has granted bioRxiv a license to display the preprint in perpetuity. It is made available under aCC-BY 4.0 International license.

AUTHOR SUMMARY

Vector-borne diseases account for 17% of the global burden of all infection diseases and only malaria kills nearly 500,000 individuals per year, most of them children. Climate change is impacting the geographical distribution and incidence of these diseases, therefore novel ecological-friendly strategies for vector control are needed. Here, we adapted methodologies to study fungal melanogenesis and used them to explore the melanin-based immune response of *Anopheles gambiae* against malaria parasites. We revealed that pheomelanin together with eumelanin is incorporated in the melanotic capsules against *Plasmodium.* We also found that melanin-encapsulated *Plasmodium* is associated to acid-resistant mosquito gut proteins and identify several putative factors of the melanin-mediated immunity. Disruption of a surface-associated protein, found highly conserved among other mosquito vectors, demonstrates its ability to impaired parasite development within the mosquito gut. Our study provides a new approach to investigate the melanin-based defense mechanism in insects, which identified a new host molecule as a potential avenue for developing novel universal pest management schemes.

INTRODUCTION

Malaria is a devastating parasitic disease that has afflicted humans since ancient times. Globally, it is responsible for approximately half-million deaths per year, 90% of them occurring in Sub-Saharan Africa, and mostly in children less than 5 years of age [1]. The disease is caused by *Plasmodium* parasites, which must undergo a complex developmental cycle inside a mammalian host and an obligatory insect vector, the anopheline mosquitoes [2]. Mosquito midgut

bioRxiv preprint doi: https://doi.org/10.1101/2021.05.07.443077; this version posted May 8, 2021. The copyright holder for this preprint (which was not certified by peer review) is the author/funder, who has granted bioRxiv a license to display the preprint in perpetuity. It is made available under aCC-BY 4.0 International license.

71 infection by *Plasmodium* motile ookinetes and their subsequent differentiation into oocysts
72 (encysted form) is a crucial stage for successful parasite development and malaria transmission
73 [3]. Several reports have demonstrated that ookinetes establish multiple protein-protein and
74 protein-glycan interactions with surface molecules of the midgut epithelial cells to mediate their
75 adhesion, attachment, and invasion [4-8]. Conversely, during the parasite's development in the
76 mosquito gut, it is targeted by innate immune defenses that rely on systemic and cellular effector
77 mechanisms mediating parasite killing; the midgut is therefore regarded as a bottleneck in the
78 malaria transmission cycle [9, 10]. A major defense system against invading pathogens is the
79 melanin-based immune response which also can target *Plasmodium* during the ookinete traversal
80 of the midgut epithelium, albeit this defense is rarely observed in natural infections with
81 *Plasmodium* [11] because of parasite immune-evasive mechanisms [12-14].

82 Melanins are high molecular weight, insoluble, and acid-resistant biopolymers that exhibit a
83 stable free radical signature [15]. These pigments are found across all kingdoms of life and play
84 key roles in diverse physiological processes of insects, such as cuticle hardening, wound healing,
85 eggshell resistance to desiccation, and immune defenses (reviewed in [16]). As a defense
86 mechanism, melanization is the result of an enzymatic reaction that oxidizes tyrosine into melanin
87 precursors followed by additional oxidation and crosslinking to proteins. This results in the
88 formation of melanotic capsules, melanin-layered structures that surround and sequester invading
89 pathogens [17]. The melanin biosynthesis pathway involves a multistep proteolytic cascade that
90 turns pro-phenoloxidases (PPOs) zymogens into active phenoloxidases (POs), which generate free
91 radicals and toxic quinone intermediate radicals as secondary metabolites. PPO enzymes are stored
92 in both circulating and sessile hemocytes (insect immune cells), which play a central role in
93 melanogenesis (reviewed in [18]). Unlike mammals and fungi, where the melanization reaction is

bioRxiv preprint doi: https://doi.org/10.1101/2021.05.07.443077; this version posted May 8, 2021. The copyright holder for this preprint (which was not certified by peer review) is the author/funder, who has granted bioRxiv a license to display the preprint in perpetuity. It is made available under aCC-BY 4.0 International license.

compartmentalized within a vesicle called melanosome [19-21], defense-mediated melanization in insects occurs in an infected body cavity, and consequently requires tight regulation to avoid the deleterious effects of toxic by-products. To restrict damage, several invertebrates have developed an alternative strategy. POs can form activation complexes associated with a functional amyloid-scaffold, which provides a site-specific to sequester and accelerate melanin precursor polymerization, anchor melanin, and promote hemocytes adhesion during the pathogen encapsulation [22-24]. In malaria-transmitting mosquitoes the complex and tightly regulated process of pathogen recognition by the complement-like protein TEP1, responsible for the elimination of *Plasmodium* ookinetes through lysis or melanization, has been extensively documented [25-27]; however, the factors and mechanism(s) mediating melanin accumulation and hemocyte recruitment to successfully target the pathogen surfaces and minimize damage to the host, are poorly understood. Current knowledge about melanin-related defenses in insects suggest that formation of a functional amyloid-scaffold is required for enhanced melanin accumulation and anchorage upon hemocyte-targeted intruders [22, 28].

Previously, we have used the environmental fungus *Cryptococcus neoformans* as a model to study melanin biology and demonstrated that fungal cell-wall constituents like chitin, chitosan, and lipids serve as scaffolding for melanin accumulation [29-31], while the melanin granules themselves are intimately associated to proteins that may be essential in the synthesis and/or structure of the biopolymer [19]. Here, we adapted protocols developed to study fungal melanization and used them to investigate the biophysical nature of melanotic capsules to explore the hypothesis that these structures will trap key mosquito factors involved in establishing the melanin-based immune response against malaria parasites and/or mediating parasite interaction with the midgut epithelium.

bioRxiv preprint doi: https://doi.org/10.1101/2021.05.07.443077; this version posted May 8, 2021. The copyright holder for this preprint (which was not certified by peer review) is the author/funder, who has granted bioRxiv a license to display the preprint in perpetuity. It is made available under aCC-BY 4.0 International license.

RESULTS

Melanotic capsules of *Anopheles* mosquito against malaria parasites are made of eumelanin and pheomelanin. The genetically selected *A. gambiae* L3-5 refractory (R) strain is known to melanize most *P. berghei* parasites in the midgut epithelium because of a dysregulated redox system [32, 33]. In this study, for the ease of accumulation of melanotic capsules, we have used this model system. To isolate melanized *Plasmodium* parasites from infected mosquito midguts, we employed a modification of the protocol used to obtain "melanin ghosts" from fungal cells, that relies on the acid-resistant property of melanin [34, 35]. This property was critical for obtaining the melanized sample material that we further analyzed as illustrated in (**Figure 1A**). As the tissues were digested by acid exposure, examination of remaining material by light microscopy demonstrated the recovery of a dark-colored material that tended to clump together (**Figure 1B, top; Figure S1)**. The acid-resistant aggregates were analyzed by dynamic light scattering (DLS), which revealed particles with a mean diameter of 1283.8 nm and 2015.1 nm, at 30- and 60-min post-treatment, respectively, consistent with the size dimensions observed by microscopy. The formation of aggregates correlated with the tough and highly hydrophobic nature of melanins (**Figure 1B, bottom**). Further studies by scanning electron microscopy (SEM) showed that the aggregated material corresponded to masses of clumped ookinetes (**Figure 1C**), while a cross-sectional micrograph visualized by transmission electron microscopy (TEM) revealed a single ookinete coated by an electron-dense material with granular appearance highly suggestive of melanin (**Figure 1D**).

bioRxiv preprint doi: https://doi.org/10.1101/2021.05.07.443077; this version posted May 8, 2021. The copyright holder for this preprint (which was not certified by peer review) is the author/funder, who has granted bioRxiv a license to display the preprint in perpetuity. It is made available under aCC-BY 4.0 International license.

Insect melanotic capsules are assumed to be composed of melanin but this assumption has not been experimentally validated by direct characterization of these structures. Consequently, we examined the physicochemical nature of the aggregated material by optical absorption and fourier transform infrared spectroscopy (FTIR). A well-dispersed suspension of isolated melanotic capsules exhibited the classical monotonic, featureless, and broad band UV-visible spectrum (**Figure 1E**), similarly to those reported for *C. neoformans* and synthetic melanins [36, 37]. The infrared spectrum of the previously isolated material was a characterized by: 1) a broad absorption band at 3200 cm^{-1}, which reflects stretching vibrations of –OH and $–NH_2$ groups [38]; 2) bands centered around 2930 cm^{-1} corresponding to vibrations of CH_2 and CH_3 aliphatic groups [39]; 3) strong absorption bands at 1600 cm^{-1} assigned to the vibrations of aromatic groups (C=O or C=C), which are typically seen for a conjugated quinoid structure and represent a key feature for the identification of melanins; and 4) weak absorption bands between 700-600 cm^{-1} due to C-S stretching vibration, suggesting of presence of pheomelanin [40, 41] (**Figure 1F**). Except for the last absorption bands corresponding to sulfur groups, all other bands are like those found in *C. neoformans* eumelanin (**Figure 1F**).

Altogether, these analyses demonstrate that the melanin-based immune response of *A. gambiae* mosquitoes against malaria parasites requires synthesis and assembly of a granular polymer composed of both eumelanin and pheomelanin. To our knowledge, this is the first experimental evidence of pheomelanin incorporation together with eumelanin in the insect immune defense mechanism triggering melanotic encapsulation.

Identification of acid-resistant proteins enriched in *Plasmodium*-infected midguts from *A. gambiae*'s melanotic capsules. We further explored whether a proteomic analysis of melanin-

bioRxiv preprint doi: https://doi.org/10.1101/2021.05.07.443077; this version posted May 8, 2021. The copyright holder for this preprint (which was not certified by peer review) is the author/funder, who has granted bioRxiv a license to display the preprint in perpetuity. It is made available under aCC-BY 4.0 International license.

encapsulated parasites allowed us to identify mosquito proteins involved in the establishment of the melanin-based immune response and/or mediating parasite interaction with the midgut epithelium to promote its invasion. To distinguish proteins associated to the mosquito melanin-based immune response, we aimed to identify proteins that were found enriched in midguts of mosquitoes fed with a *P. berghei*-infected bloodmeal in comparison to midguts from naïve blood fed mosquitoes, before and after incubation in acid.

As expected, homogenates from midgut tissues infected with malaria parasites exhibited a different pattern of total proteins in comparison to the homogenates from naïve blood-fed midguts prior to acid treatment (**Figure 2A**). In contrast, after acid digestion the total protein content for both samples was significantly reduced but a subtle smear was still noticeable demonstrating that a small number of proteins were resistant to acid degradation (**Figure 2A, top**). Following solubilization of proteins from midgut tissues and using a filter-aided sample preparation (FASP)-based procedure coupled with mass spectrometric analyses allowed us to identify three sets of proteins enriched in the infected sample vs control: **A)** Pre-acid treatment; **B)** Post-acid treatment; and **C)** Subset commonly found pre- and post-acid treatment (**Figure 2A, bottom**). Before the acid hydrolysis, proteomic analysis identified 336 proteins enriched in response to *Plasmodium* infection. According to the top ten gene ontology (GO) terms related to biological process, many of these proteins are involved in cell redox-homeostasis, response to oxidative stress, and aerobic respiration (**Table S1**), which correlates with the elevated generation of mitochondrial reactive oxygen species (ROS) previously reported for *A. gambiae* R strain [33, 42]. After the acid treatment, a subset of 14 acid-resistant proteins enriched in infected midguts was identified, suggesting that these were shielded from acid degradation by a close association with melanin (**Figure 2B, Table S2**). According to their cellular localization, 79% are intracellular proteins (*N*

bioRxiv preprint doi: https://doi.org/10.1101/2021.05.07.443077; this version posted May 8, 2021. The copyright holder for this preprint (which was not certified by peer review) is the author/funder, who has granted bioRxiv a license to display the preprint in perpetuity. It is made available under aCC-BY 4.0 International license.

185 = 11) likely found in the cytoplasm (*N* = 2), associated to membranes (*N* = 4) or to the cytoskeleton
186 (*N* = 2), while the remaining 21% (*N* = 3) correspond to extracellular proteins (**Figure 2B,**
187 **unshadowed area**). Only protein (AGAP004742) was found enriched in both conditions. Notably,
188 the 3 extracellular proteins embedded within *Anopheles* melanotic capsules are surface-associated
189 molecules [AGAP000550 (AMOP, complement module), AGAP007745 (Peritrophic matrix-
190 associated protein), AGAP010479 (*Ag*EBP)] previously reported as potential targets of
191 transmission-blocking vaccine (TBV) [8, 43, 44].
192
193 ***Ag*Mesh (AGAP000550) influences malaria parasite development.** Multiple molecules on the
194 midgut surface are shown to play critical roles in the process of midgut adhesion and invasion by
195 *Plasmodium* parasites [4-7, 43]. An in-silico analysis on the above 3 proteins has identified one
196 interesting protein for further investigation. The complete sequence of AGAP000550 reveals a
197 single transcript size of 6.08 kb and a predicted 1,407-amino acid polypeptide of unknown
198 function. It shares high amino acid sequence identity across main anophelines vectors of malaria
199 (> 86%) and other vectors of arboviruses *Aedes aegypti* and *Aedes albopictus* (~78%) (**Figure**
200 **3A).** Its predicted protein sequence contains multiple domains that have been previously found in
201 various immune factors, such as an immunoglobulin domain [43], NIDO, AMOP, von Willebrand
202 factor type D (VWFD), and CCP (complement control protein) also known as short complement-
203 like repeat or SUSHI repeats (**Figure 3B**). These domains are also identical to those identified in
204 *Drosophila melanogaster* Mesh (CG31004), a transmembrane protein critical for the formation
205 and barrier function of septate junctions -functional counterparts of tight junctions in vertebrates
206 [45]. Thus, we refer to AGAP000550 as *A. gambiae* Mesh (*Ag*Mesh). The high degree of
207 conservation across disease-transmitting insect vector species and its domain composition,

bioRxiv preprint doi: https://doi.org/10.1101/2021.05.07.443077; this version posted May 8, 2021. The copyright holder for this preprint (which was not certified by peer review) is the author/funder, who has granted bioRxiv a license to display the preprint in perpetuity. It is made available under aCC-BY 4.0 International license.

suggests the likely recognition and immune functions of *Ag*Mesh, which might play a potent role in the establishment of *Plasmodium* infection in the mosquito midgut.

To investigate whether *Ag*Mesh is influencing *Plasmodium* infection of the mosquito midgut and its association with the melanin-based immune defense, we assessed the capacity of both *P. falciparum* and *P. berghei* to establish infection in the midgut of the susceptible *A. gambiae* (Keele strain) (S) and the refractory *A. gambiae* (L3-5 strain) (R), respectively, using a RNAi-based gene silencing approach (**Figure 4**). A double-stranded RNA (dsRNA) corresponding to a 151-bp coding region of *Ag*Mesh was injected into the mosquitoes thorax to deplete *Ag*Mesh mRNA 4 days prior to infection with a *Plasmodium*-laced bloodmeal; control mosquitoes were injected with *dsGFP*, an unrelated gen. Silencing of *Ag*Mesh in the S mosquitoes resulted in a decreased (median number of oocysts 7 vs 13, $p = 0.0002$) *P. falciparum* infection intensity compared to the ds*GFP*-injected (**Figure 4A, left**), whereas the infection prevalence was not affected (90% vs 95%) (**Figure 4B, left).** Depletion of *Ag*Mesh in the R strain resulted in a decreased *P. berghei* infection intensity and prevalence in comparison to control in comparison to control [median number of total parasites 2 vs 12, $p < 0.0001$ (**Figure 4A, right**); prevalence 44% vs 93%, $p < 0.0001$ (**Figure 4B, right**)]. Interestingly, *Ag*Mesh-silencing did not abolish the melanization phenotype in the R strain [median number of melanized parasites 2 vs 4, $p = 0.0007$ (**Figure 4C, right**)], but it significantly reduced parasite development within the midgut of both susceptible and refractory mosquitoes. The weakened melanin-based immune response in the *Ag*Mesh-silenced R mosquitoes could be due to a lesser number of ookinetes reaching the basal lamina or to a direct implication of *Ag*Mesh in the melanization process. Nevertheless, *Ag*Mesh disruption in this strain seemed to promote *Plasmodium* recognition since no midgut exhibited live parasite only in contrast to 19% in the R control (**Figure 4D**).

bioRxiv preprint doi: https://doi.org/10.1101/2021.05.07.443077; this version posted May 8, 2021. The copyright holder for this preprint (which was not certified by peer review) is the author/funder, who has granted bioRxiv a license to display the preprint in perpetuity. It is made available under aCC-BY 4.0 International license.

To gain a better understanding on the spatial specificity of AgMesh's influence on infection we assessed whether its depletion may disrupt *P. berghei* ookinete development at the luminal compartment of the midgut 26 h post infection (hpi) as well as its ability to invade the midgut tissue. An exploratory analysis of the parasite presence in the lumen was performed by dissecting midguts of AgMesh-silenced mosquitoes at 26 hpi. Visual examination with a light microscope of smears from lumen content stained with giemsa revealed several immature stages of the parasite, along with abundant gut microbiota (**Figure S2A**, red arrow heads). Immunohistochemical analyses of midgut sheets to localize parasites via detection of the ookinete surface protein P28 [46] using the anti-Pbs28 antibody were performed by confocal microcopy (**Figure S2B**). There results indicated that *P. berghei* ookinetes could successfully invade the midgut epithelial cells in *Ag*Mesh-silenced R mosquitoes. As a noteworthy observation derived from these trials was an apparent loss of gut elasticity and integrity upon *Ag*Mesh depletion, further pointing at a function of *Ag*Mesh as a structural component. Difficulties with the maintance and acquisition of the *A. gambiae* L3-5 refractory strain hindered us to conduct further experiments to elucidate the role of AgMesh in *Plasmodium* melanization.

DISCUSSION

Melanin synthesis in insects is crucial for their survival (reviewed by [16]). These natural pigments are involved in multiple physiological processes including cuticle hardening, wound healing, and innate immune response. In vector mosquitoes such as the malaria vector *A. gambiae*, the innate immune system actively restricts and neutralizes foreign organisms including those transmitted to the human host. A better understanding of the chemical nature and molecular

bioRxiv preprint doi: https://doi.org/10.1101/2021.05.07.443077; this version posted May 8, 2021. The copyright holder for this preprint (which was not certified by peer review) is the author/funder, who has granted bioRxiv a license to display the preprint in perpetuity. It is made available under aCC-BY 4.0 International license.

254 scaffolds required to establish a robust melanin-based immune response could inform the
255 development of novel strategies to block transmission of vector-borne human pathogens.

256 In this study, we explored the *A. gambiae* melanin-based immune response against malaria
257 parasites by exploiting and adapting a toolbox of multidisciplinary strategies used for the analysis
258 of *C. neoformans* melanin [19, 35]. We took advantage of melanin's ability to resist degradation
259 by acids and allowed us to isolate *A. gambiae* melanotic capsules. We then applied a range of
260 microscopic and spectroscopic analyses to investigate the physicochemical nature of these
261 particles. Lastly, we conducted a proteomic analysis to identify mosquito proteins that remained
262 crosslinked to melanin after the acid treatment. These results demonstrate that the isolated material
263 from mosquito guts in response to *Plasmodium* infection exhibited consistent properties of
264 melanin: highly hydrophobic, acid-resistant, and having a monotonic broadband absorption curve.
265 The melanin coat surrounding an ookinete revealed a unique electron microscopy appearance of
266 tightly packed nanospheres similarly to those reported for melanized cryptococcal cells after
267 extensive acid hydrolysis [19]. These melanotic capsules incorporated both eumelanins and
268 pheomelanins, therefore providing the first experimental confirmation that pheomelanins play a
269 role in insect immunity.

270 Early biochemical studies of melanogenesis in other organisms [47], deduced that melanotic
271 capsules were composed of an eumelanin and pheomelanin mixture as formation of thiols
272 conjugates from dopaquinone naturally occur 1,000 times faster that its cyclization into
273 leucodopachrome. Nonetheless, reports of sulfur-containing pheomelanins in insects are restricted
274 to cuticular pigmentation analyses in *D. melanogaster* [48], the grasshopper *Sphingonotus*
275 *azurescens* [49], species of bumblebee from the genus *Bombus* [50], and male parasitoid wasps
276 from the genus *Mesopolobus* [51]. The functional significance of pheomelanins in the immune

bioRxiv preprint doi: https://doi.org/10.1101/2021.05.07.443077; this version posted May 8, 2021. The copyright holder for this preprint (which was not certified by peer review) is the author/funder, who has granted bioRxiv a license to display the preprint in perpetuity. It is made available under aCC-BY 4.0 International license.

277 eumelanin surrounding *Plasmodium* may reflect pro-oxidant activity as well as anti-inflammatory
278 and antioxidant properties [52], respectively, to promote the parasite killing while avoiding host
279 damage. Given that dopamine is the main precursor for both eumelanin and pheomelanin in insects
280 [48], it is possible that melanotic capsules exhibit neuromelanin-like properties [53]. These
281 melanin cages may serve as a trapping system that prevents accumulation of toxic quinones
282 produced by dopamine oxidation [54]. Further chemical and structural investigations of the
283 mosquito melanin-based immune response are encouraged to further elucidate these mechanisms.
284 Malaria parasite infection has been reported to elicit extensive *A. gambiae* transcriptome
285 responses that mediate an effective control of *Plasmodium* [55]. Knowing that melanization of
286 *Plasmodium* ookinetes occurs as early at 16 h post infection (hpi) [32, 56], we decided to dissect
287 midguts 6 days post infection (dpi) to recover fully melanized parasites for our analyses. The
288 rationale for this choice was the following: a) at 32 hpi *A. gambiae* R strain kills over 90 % of
289 ookinetes, which persist melanized through the mosquito lifetime [56]; b) parasite melanization
290 occurs in parallel to two peaks of *TEP1* expression at 24 hpi and 3-4 dpi, in accordance with the
291 passage of ookinetes through the columnar cells of the midgut epithelium and the establishment
292 of oocysts, respectively [56]; and c) to avoid gross contamination of our samples with human blood
293 and serum proteins. In addition, a previous report demonstrated that mosquitoes fed on uninfected
294 blood exhibit elevated expression of immune genes in response to the expansion of the mosquito's
295 natural gut microbiota [57].
296 Melanotic capsules from *A. gambiae* against the malaria parasite demonstrated an association
297 with 14 proteins, which were found enriched in infected midguts post-acid hydrolysis, suggesting
298 a possible role on the anti-*Plasmodium* response and close localization to the melanin-coated
299 parasite. A single protein identified as pyruvate carboxylase (AGAP004742) known to be critical

bioRxiv preprint doi: https://doi.org/10.1101/2021.05.07.443077; this version posted May 8, 2021. The copyright holder for this preprint (which was not certified by peer review) is the author/funder, who has granted bioRxiv a license to display the preprint in perpetuity. It is made available under aCC-BY 4.0 International license.

300 for gluconeogenesis and fatty acid synthesis was shared among the two sets. Functional and
301 physiological studies using the melanizing *A. gambiae* R strain demonstrated that parasite
302 encapsulation is due to increased levels of reactive oxygen species which are further augmented
303 by blood feeding [58, 59]. In agreement with the dysregulation of three key biological processes
304 in this refractory mosquito strain [59], half of the acid-resistant proteins enriched in infected
305 midguts are involved in mitochondrial respiration (AGAP000881, AGAP002884, AGAP012081,
306 AGAP005134), redox-metabolism (AGAP007790, AGAP012407), and lipid metabolism
307 (AGAP004742) [42]. Two additional acid-resistant proteins (AGAP004877, AGAP010147)
308 cytoskeleton-related were also found enriched in infected midguts possibly reflecting major
309 cytoskeletal rearrangements due to blood engorgement and/or ookinete parasite invasion the
310 midgut epithelium [60, 61]. Furthermore, AGAP001151 orthologs in *D. melanogaster* [62] and
311 *Ae. aegypti* [63] (96 and 93% identity, respectively) play a critical role in the innate immune
312 response. Multiple studies have shown that *Plasmodium* melanization occurs upon ookinete
313 contact with the mosquito hemolymph when the parasite reaches the basal side of the epithelial
314 cells [32, 56, 64, 65]; our finding of previously reported extracellular surface-associated molecules
315 (AGAP000550, AGAP007745, AGAP010479) in close association with the melanotic capsules
316 was in agreement with these earlier studies. Nonetheless, a recently published live *in vivo* imaging
317 of *Plasmodium* invasion of the mosquito midgut clearly depicted three stages of this process: i)
318 lumen localization; ii) contact with the microvillar surface, and iii) cell invasion [60]. Hence,
319 "parasite coating" with the identified surface components was not unexpected. AGAP010479
320 (*Ag*EBP) [8] is known to be important ookinete-interacting proteins that mediate midgut invasion
321 through its apical side. AGAP007745 is an abundant peritrophic matrix (PM)-associated protein
322 predicted to be heavily glycosylated and containing a proline-rich domain, which may play a

bioRxiv preprint doi: https://doi.org/10.1101/2021.05.07.443077; this version posted May 8, 2021. The copyright holder for this preprint (which was not certified by peer review) is the author/funder, who has granted bioRxiv a license to display the preprint in perpetuity. It is made available under aCC-BY 4.0 International license.

323 structural role in the PM [44]. AGAP000550 (*Ag*Mesh) is a secreted uncharacterized mucin-related
324 protein also found associated with the midgut brush border microvilli (BBMV) proteome of *A.*
325 *gambiae* and *A. albimanus* [43, 66]. Its extracellular domains NIDO and AMOP are found in cell
326 adhesion molecules possibly mediated by the presence of cysteines and tyrosine residues involved
327 in disulfide and dityrosine bonds, respectively. The mucin VWFD is required for blood clotting
328 factor VIII binding and normal multimerization of VWF [67, 68]. Interestingly, phenoloxidases
329 are humoral procoagulants that catalyze clot hardening serving both immune and structural
330 functions [reviewed in [24]]. Furthermore, SUSHI (CCP) is an evolutionary conserved domain
331 essential for complement-mediated immune functions and plays an important role in insect-
332 microbe interactions [69]. We showed that *Ag*Mesh silencing in both *A. gambiae* S and R female
333 mosquitoes significantly reduced their susceptibility to the malaria parasite infection. Particularly
334 in the R strain, Mesh-silenced mosquitoes exhibited a 2-fold decreased of parasite ookinete
335 melanization and severe impairment of parasite development within the midgut epithelium.
336 Many hematophagous insects including *A. gambiae* are known to control overproliferation of
337 commensal microbiota via dual oxidase (Duox) activity at midgut epithelium in response to a
338 bloodmeal [70-72]. Duox is a transmembrane protein that contributes to gut homeostasis by
339 secreting ROS [73] and promoting the formation of a dityrosine network (DTN) that stabilizes the
340 peritrophic membrane (PM) [74, 75]. The PM is an acellular semipermeable layer composed of
341 chitin polymers. In *A. gambiae*, a Duox/Peroxidase (IMPer) system catalyzes formation of the
342 DTN by protein cross-linking in the mucin layer, which is in the ectoperitrophic space between
343 the PM and the midgut epithelium [71, 76]. The DTN forms a permeability barrier that prevents
344 immune responses of mosquito epithelial cells against gut microbiota, thus favoring *Plasmodium*
345 parasites development in the midgut lumen. Based on the results obtained in this study, we

bioRxiv preprint doi: https://doi.org/10.1101/2021.05.07.443077; this version posted May 8, 2021. The copyright holder for this preprint (which was not certified by peer review) is the author/funder, who has granted bioRxiv a license to display the preprint in perpetuity. It is made available under aCC-BY 4.0 International license.

346 hypothesize that tyrosine residues from extracellular domains NIDO and AMOP of *Ag*Mesh serve
347 as substrate to Duox/IMPer to form covalent dityrosine bonds that give rise to the DTN. Reduced
348 parasite infection exhibited in S and R *Ag*Mesh-silenced mosquitoes may be due to a sustained
349 induction of microbicidal effector genes as PM integrity has been compromised as it was
350 demonstrated when either Duox or IMPer are silenced [71]. The enhanced levels of ROS and
351 chronic state of oxidative stress known for the R strain [58, 59] could explain the stronger decrease
352 of parasite intensity and no ability of *Plasmodium* to develop inadvertently, which was evidenced
353 by the absence of midguts only exhibiting live oocysts. The lack of PM integrity could also
354 correlate with the fragility noticed on blood-filled guts of *Ag*Mesh-silenced mosquitoes at 26 hpi
355 possible related to a dysregulation of the gut microbiota homeostasis [77, 78]. Furthermore,
356 *Ag*Mesh AMOP domain contains 8 invariant cysteine residues predicted to be involved in the
357 formation of intermolecular disulfide bonds suggesting a beta-sheet organization and possible
358 protein multimerization [79, 80]. *Ag*Mesh mucoid-coating of those parasite ookinetes that
359 successfully invaded the gut epithelium and reached the basal lamina could serve as a molecular
360 scaffold (amyloid-like) mediating deposition and accumulation of the site-specific melanin-based
361 immune response. This hypothetical model provides a rational explanation for *Ag*Mesh association
362 with the mosquitoes melanotic capsules. The absence or reduction of *Ag*Mesh avoids formation of
363 the dityrosine-based barrier therefore increasing gut permeability and diffusion of immune elicitors
364 triggering the host immune defenses against *Plasmodium* parasites. Additional analyses to validate
365 this theory are being performed using the *A. gambiae* G3, parental strain of L3-5.

366 Our experimental approach to investigating components associated with insect melanotic
367 capsules was inspired by the success of similar work in melanotic yeasts [19]. The ability of
368 melanin to resist acid digestion allows its recovery in granular form and our results show that it is

bioRxiv preprint doi: https://doi.org/10.1101/2021.05.07.443077; this version posted May 8, 2021. The copyright holder for this preprint (which was not certified by peer review) is the author/funder, who has granted bioRxiv a license to display the preprint in perpetuity. It is made available under aCC-BY 4.0 International license.

associated with numerous proteins. We caution that close association does not necessarily imply a role in either melanotic capsule formation or host defense. However, the fact that these proteins resisted acid digestion does imply some form of tight linkage, or protection by the melanin pigment, which in turn hints at a possible involvement in host defense or *Plasmodium* pathogenesis. By choosing one of these proteins with unknown function and then showing that interference with its expression in mosquitoes reduced *Plasmodium* spp. infection, our results provide a proof of principle that this approach can lead to proteins involved in process of parasite infection.

In summary, our analysis provides a new approach to the study of the *A. gambiae* melanin-based immune response against malaria parasites by characterizing the melanotic capsule and by identifying several candidate factors of melanin-mediated immunity. The high degree of *Ag*Mesh conservation across mosquito vectors of human diseases and its influence on *Plasmodium* infection suggests it may represent a fertile line of investigation in the search of a universal transmission-blocking strategy, which aims to target the PM for insect pest management. Lastly, the striking resemblances in the molecular scaffolding of polyaromatic polymers (dityrosine and melanin) that are conserved in insects as well as in the fungal kingdom [81], highlight the functional importance for these dark pigments in the tree of life.

MATERIALS AND METHODS

Ethics statement. This project was carried out in accordance with the recommendations of the Guide for the Care and Use of Laboratory Animals of National Institutes of Health. The animal protocols and procedures were approved by the Animal Care and Use Committee of the Johns

bioRxiv preprint doi: https://doi.org/10.1101/2021.05.07.443077; this version posted May 8, 2021. The copyright holder for this preprint (which was not certified by peer review) is the author/funder, who has granted bioRxiv a license to display the preprint in perpetuity. It is made available under aCC-BY 4.0 International license.

Hopkins University (Protocol MO15H144). Commercial anonymous human blood was used for parasite cultures and mosquito feeding, no informed consent was required.

Biological materials. *Plasmodium berghei* (ANKA clone 2.34) were propagated in random-bred Swiss Webster female mice. *P. falciparum* NF54 (Walter Reed National Military Medical Center, Bethesda) infectious gametocyte cultures were provided by the Johns Hopkins Malaria Research Institute Parasite Core Facility and were diluted to 0.03% gametocytemia before feeding to the mosquitoes using an artificial membrane feeder. *Anopheles gambiae* L3-5 strain and *A. gambiae* Keele strain mosquitoes were maintained on sugar solution at 27 °C and 70% humidity with a 12-h light to dark cycle according to standard rearing condition.

Isolation of melanotic capsules from mosquito midguts. *A. gambiae* L3-5 strain female mosquitoes were infected with *P. berghei* (ANKA clone 2.34) by feeding them on an anesthetized infected mouse. The infectivity of each mouse was established by measuring the parasitemia and visualizing 1-2 exflagellation events/field under the microscope. Blood-fed mosquitoes were kept at 19 °C for 6 d to allow parasite ookinetes invasion of midgut epithelial and development of the mosquito melanin-based anti-*Plasmodium* immune response. Around 200 midguts were dissected in Dulbecco's phosphate-buffered saline (DPBS) (Corning), transfer to a 5ml-tube containing 75% ethanol while avoiding contamination from other mosquito body parts (ovaries, thorax, legs, wings, and head), and kept at 4 °C. Dissected guts were washed two times with DPBS and resuspended in distilled water. Midguts were homogenized by sequentially aspirating them through a 26-gauge and 27-gauge needle, 10 times each. Homogenized material (~500 µl) was transferred to a 1.5-ml tube and an equal volume of 12 N HCl was added. Using a Thermomixer

bioRxiv preprint doi: https://doi.org/10.1101/2021.05.07.443077; this version posted May 8, 2021. The copyright holder for this preprint (which was not certified by peer review) is the author/funder, who has granted bioRxiv a license to display the preprint in perpetuity. It is made available under aCC-BY 4.0 International license.

C (Eppendorf AG, Germany), homogenate suspended in distilled water was incubated at 80 °C with 800 rpm shaking speed. Aliquots were removed at 5, 10, 20, 30, 40, 50, 60 min, transferred to a clean tube, and centrifuged at 45,000 rpm for 5 min. The pellet from each aliquot, corresponding to melanin aggregates, was resuspended in 50 µl DPBS and examined under a light-contrast microscope.

Dynamic Light Scattering (DLS). DLS is a non-destructive physical technique that provides information on the size and heterogeneity of a sample by measuring the random fluctuations of scattered light by particles in suspension. Measurement of melanin aggregates particles formed along the melanotic capsules isolation was performed with a 90Plus/BI-MAS Multi Angle particle size analyzer (Brookhaven Instruments). Thus, 10 µl of melanin aggregates suspension was diluted to 100 µl in DPBS. Data are expressed as the average of 10 runs of 1-min data collection each. Particle size distribution by number emphasized the smaller size in the sample, reflecting melanin hydrophobicity and aggregation as exposure time to acid increased.

Electron Microscopy. A 50 µl aliquot of melanin aggregates recovered from *A. gambiae* infected midguts after 60 min of incubation in 6 M HCl was fixed in 2.5% (v/v) glutaraldehyde, 3mM $MgCl_2$ in 0.1 M sodium cacodylate buffer, pH 7.2 for 1 h at room temperature. For TEM, after buffer rinse, samples were post-fixed in 1% osmium tetroxide, 0.8% potassium ferrocyanide in 0.1 M sodium cacodylate for at least 1 h (no more than two) on ice in the dark. After osmium, samples were rinsed in 100 mM maleate buffer, followed by uranyl acetate (2%) in 100 mM maleate (0.22 µm filtered, 1 h, dark), dehydrated in a graded series of ethanol and embedded in Eponate 12 (Ted Pella) resin. Samples were polymerized at 37 ^{o}C for 2-3 days followed by 60 ^{o}C overnight. Thin

bioRxiv preprint doi: https://doi.org/10.1101/2021.05.07.443077; this version posted May 8, 2021. The copyright holder for this preprint (which was not certified by peer review) is the author/funder, who has granted bioRxiv a license to display the preprint in perpetuity. It is made available under aCC-BY 4.0 International license.

438 sections, 60 to 90 nm, were cut with a diamond knife on the Reichert-Jung Ultracut E
439 ultramicrotome and picked up with 2x1 mm formvar copper slot grids. Grids were stained with
440 2% uranyl acetate in 50% methanol followed by lead citrate and observed with a Philips CM120
441 TEM at 80 kV. Images were captured with an AMT CCD XR80 (8 Megapixel camera - side mount
442 AMT XR80 – high-resolution high-speed camera). For SEM, samples were fixed and rinsed as
443 described above. After buffer rinse, samples were post-fixed in 1% osmium tetroxide in 0.1 M
444 sodium cacodylate buffer (1 h) on ice in the dark. Following a DH_2O rinse, samples were
445 dehydrated in a graded series of ethanol and left to dry overnight (in a desiccator) with
446 hexamethyldisilazane (HMDS). Samples were mounted on carbon coated stubs and imaged on the
447 Zeiss Leo FESEM (Field Emission Scanning Electron Microscope) at 1kV.
448
449 **Fourier-transform Infrared Spectra (FTIR).** A dry sample (~ 2 mg) of melanin aggregates
450 recovered from *A. gambiae* infected midguts after 60 min of incubation in 6 M HCl were IR
451 characterized using a Nicolet Nexus 670 FT-IR spectrometer coupled with Smart Gold Gate KRS-
452 5 accessory (Thermo Fisher Scientific, USA). FTIR spectra were recorded between 4000 and 400
453 cm^{-1} in transmittance mode averaging 32 scans. Spectra resolution was 4 cm^{-1}. A standard
454 eumelanin spectrum was also obtained using *Cryptococcus neoformans* melanin. Data acquisition
455 was done using OMNIC software (Thermo Fisher Scientific).
456
457 **RNA interference (RNAi) gene-silencing.** Primers specific to *AgMesh* (**Table S3**) were designed
458 with the T7 polymerase promoter sequence appended to the 5'end of each oligo (5'-
459 TAATACGACTCACTATAGGG-3'). PCR products were purified, and their size verified by
460 agarose gel electrophoresis. Around 1 µg of each PCR product was used as template for dsRNA
461 synthesis using the HiScribe T7 High Yield RNA synthesis kit (New England BioLabs, Cat #

bioRxiv preprint doi: https://doi.org/10.1101/2021.05.07.443077; this version posted May 8, 2021. The copyright holder for this preprint (which was not certified by peer review) is the author/funder, who has granted bioRxiv a license to display the preprint in perpetuity. It is made available under aCC-BY 4.0 International license.

462 E2040S) as per the manufacturer's protocol. dsRNA samples were adjusted to a final concentration
463 of 3.0 µg/µl in water. *A. gambiae* female mosquitoes (3-4 d old) were cold-anesthetized and
464 inoculated intrathoracically with 69 nl of dsRNA using a nano-injector (Nanoject, Drummond
465 Scientific, USA). Mosquitoes were maintained at 19 °C for 3 d before infecting with a blood meal.
466 As control, age-matched female mosquitoes were injected with equivalent concentration of GFP
467 (green fluorescent protein gene) dsRNA. Gene silencing was verified 3 to 4 d after dsRNA
468 injection by real-time quantitative RT-PCR, done in triplicate, with the *A. gambiae* ribosomal S7
469 gene as the internal control for normalization as previously has been published [57].
470
471 ***Plasmodium* infection.** *A. gambiae* Keele strain female mosquitoes were infected artificially by
472 membrane feeding with *P. falciparum* NF54 gametocyte cultures according to an established
473 protocol [55]. The cultures were washed and diluted to 0.03% gametocytemia in normal 60%
474 human serum plus 40% human RBCs. Infected blood meal was provided to mosquitoes directly
475 from glass, water-jacketed membrane feeders warmed at 37 °C. Mosquitoes were allowed to feed
476 for 30 min, afterward unfed females were removed. Mosquitoes were kept for 8 days at 27 °C to
477 assess parasite infection by oocyst counting.
478 *A. gambiae* L3-5 strain female mosquitoes were infected with *P. berghei* (ANKA clone 2.34) as
479 described previously [55]. Blood-fed mosquitoes were kept at 19 °C for 10 d for oocyst and
480 melanized parasite counting. Midguts were dissected in DPBS (Corning) and stained in 0.2% (w/v)
481 mercurochrome to visualize parasite forms under a light-contrast microscope.
482
483 **Solubilization of proteins associated with melanotic capsules.** For the identification of proteins
484 enriched in *Plasmodium*-infected midguts and crosslinked with the melanin matrix, sample

bioRxiv preprint doi: https://doi.org/10.1101/2021.05.07.443077; this version posted May 8, 2021. The copyright holder for this preprint (which was not certified by peer review) is the author/funder, who has granted bioRxiv a license to display the preprint in perpetuity. It is made available under aCC-BY 4.0 International license.

485 homogenate was incubated in the acid solution at 80 °C for 30 min as described previously. To
486 neutralize pH, samples were centrifuged at 45,000 rpm for 30 min at 4 °C and resuspended in 2 ml
487 1M Tris-HCl. Next, sample was washed sequentially with 0.1 M Tris-HCl and PBS, three times
488 per wash with 2 volume of each solution. To solubilize melanin-associated proteins, material was
489 resuspended in 50 µl 2% SDS (end concentration) and incubate in ThermoMixer C (Eppendorf
490 AG, Germany) at 55 °C for 3 h. An aliquot of 5 µl was assess by SDS-PAGE and remaining sample
491 was submitted to the Mass Spectrometry and Proteomic Core Facility (Johns Hopkins Medicine,
492 Baltimore, MD). An enrichment approach to identify proteins expressed in response to the parasite
493 infection was conducted, using as control naïve blood-filled midguts previous and post acid
494 treatment.
495
496 **LC-MS/MS analysis**
497 Solubilization of proteins associated with the melanin matrix was facilitated by previous treatment
498 with 2% SDS (end concentration). Further studies using a filter-aided sample preparation (FASP)-
499 based procedure was conducted at the Johns Hopkins Mass Spectrometry and Proteomic Facility.
500 To each sample 40 µl of 20 mM ammonium bicarbonate pH 8.0 was added then reduced using 5
501 µl of 50 mM dithiothreitol for 1 h at 60 °C. Samples were chilled on ice then alkylated using 5 µl
502 of 50 mM iodoacetamide for 15 min in the dark. Samples were then diluted in 400 µl of 9 M
503 sequencing grade urea (Thermo Fisher). For each sample, a 30 kD MWCO spin filter (Amicon)
504 was washed with 300 µl distilled water 3 times using a centrifuge at 14,000 g for 3 min. Each
505 sample was then added to a washed spin filter and spun down at 14,000 *g* for 5 min. Two successive
506 washes with 400 µl 9 M urea were spun through each filter allowing the SDS in urea to flow
507 through the spin filter. Three additional washes with 400 µl of 20 mM ammonium bicarbonate

bioRxiv preprint doi: https://doi.org/10.1101/2021.05.07.443077; this version posted May 8, 2021. The copyright holder for this preprint (which was not certified by peer review) is the author/funder, who has granted bioRxiv a license to display the preprint in perpetuity. It is made available under aCC-BY 4.0 International license.

were used to rinse the urea from the sample prior to trypsinization. To each filter a calculated ratio of 1/50 enzyme to protein in 300 µl of 20 mM ammonium bicarbonate was added and allowed to digest at 37 °C on filter overnight. The next day, samples were each centrifuged at 14,000 *g* and the flow through of digested peptides was collected. Filters were then rinsed twice with 20 mM ammonium bicarbonate and the flow through added to the digested peptides. The peptides were then acidified and desalted on an Oasis HLB microelution plate (Waters) according to protocol. After FASP digestion, samples were brought up in 2 % acetonitrile, 0.1 % formic acid and separated with an EasyLC into a QE-Plus (Thermo Fisher Scientific) mass spectrometer and eluted over a 90-min gradient from 100% buffer A (2% acetonitrile, 0.1% formic acid) to 100% buffer B (90% acetonitrile, 0.1% formic acid) with an MS resolution of 70,000 and an MS2 resolution of 35,000 running a top 15 DDA method.

MS/MS Data analysis

Data were searched against a database compiled from the ReqSeq 2015 database entries for Anopheles gambiae (AgamP4, VectorBase) and Plasmodium berghei (downloaded October 10, 2016) using Proteome Discoverer (version 1.4) and the search engine Mascot (version 2.5.1). The enzyme designation was set to trypsin with one allowed missed cleavage and a mass tolerance of 5 ppm for precursors and 0.02 daltons for fragment ions was used. Variable modifications were allowed for M oxidation and deamidation on N and Q. Carbamidomethyl on C was set to static. The search results were filtered at a 1% FDR using the target/decoy PSM validator for peptides associated with the reported proteins. Scaffold (version 4.10.0, Proteome Software Inc, Portland, OR) was used to validate MS/MS based peptide and protein identifications. Peptide identifications were accepted if they could be established at a greater than 95.0% probability by the Peptide

bioRxiv preprint doi: https://doi.org/10.1101/2021.05.07.443077; this version posted May 8, 2021. The copyright holder for this preprint (which was not certified by peer review) is the author/funder, who has granted bioRxiv a license to display the preprint in perpetuity. It is made available under aCC-BY 4.0 International license.

Prophet algorithm [82] and contained at least 2 identified peptides. Normalized total spectral counts from each independent experiment was exported to Microsoft Excel for Windows 365 for analysis. Abundance of expressed proteins identified in control and infected samples was performed based on their consistent detection (at least 2 times across 5 independent experiments) in both experimental conditions (prior and post-acid treatment). This led to the inclusion of 336 and 14 from a total of 1110 proteins for the pre- and post-acid treatment conditions, respectively. Manual annotation of proteins found enriched in infected samples was performed using the conserved domains as predicted by VectorBase (VB-2016-2020), InterPro, Pfam, UniProt, and BLAST. Previous literature regarding genomic analyses of *A. gambiae*, particularly of the L3-5 strain, were also used as reference [42, 58].

In silico analysis

Bioinformatic analysis to identify predicted domain structures was conducted using PROSITE MyDomains [83]. To estimate amino acid sequences percentage identity analysis was conducted using Geneious Prime Software (version 2020.1.2). Proteomic data were visualized and analyzed using the Scaffold Proteome Software (version 4.10.0).

Statistical analysis

GraphPad Prism 9 (version 9.0.2) software package was used to performed statistical analyses. Test used in a particular experiment is indicated in its respective Figure legend.

Figure 1. Isolation and characterization of melanotic capsules of _Anopheles_ mosquitoes infected with _Plasmodium_ spp. A, Workflow and experimental scheme. **B, Top,** Time-course

bioRxiv preprint doi: https://doi.org/10.1101/2021.05.07.443077; this version posted May 8, 2021. The copyright holder for this preprint (which was not certified by peer review) is the author/funder, who has granted bioRxiv a license to display the preprint in perpetuity. It is made available under aCC-BY 4.0 International license.

554 isolation of *Anopheles* melanotic capsules during acid treatment and heating at 80˚C. Light
555 microscopy images at 100X (oil immersion) of selected time points showing acid-resistant and
556 heat-stable aggregated melanin-like material. Bar 10 μm. **Bottom,** Size of melanin aggregates
557 measured by dynamic light scattering (DLS). **C,** Scanning electron microscopy image suggestive
558 of clumped melanized *Plasmodium* ookinetes. Bar 2 μm. **D,** Cross-sectional transmission electron
559 microscopy image suggestive of melanized *Plasmodium* ookinete. Bar 500 nm (inset, 100 nm). **E,**
560 Monotonic broadband UV-visible absorption spectra of melanins. **F,** Fourier-transform infrared
561 (FTIR) spectra of fungal eumelanin from *Cryptococcus neoformans* (Top), and *A. gambiae*
562 melanotic capsules (Bottom) displaying signals corresponding to sulfur groups commonly found
563 in pheomelanins (black arrow). Both spectra were recorded in transmittance mode averaging of 32
564 scans.
565
566 **Figure 2. Proteins from *A. gambiae* infected with *Plasmodium* parasites are found in close**
567 **association with melanin capsules. A**, **Left,** SDS-PAGE Silver stained 4-12% gel of solubilized
568 midgut proteins from *A. gambiae* in response to malaria parasites. Naïve blood-fed midguts
569 homogenate (C) and *P. berghei*-infected midguts homogenate (*Pb*-inf), respectively, without HCl
570 treatment and post-30 min acid treatment. MW, Pre-stained protein molecular ladder. **A, Right,**
571 Venn diagram comparisons of proteins identities from 5 independent biological replicates of *A.*
572 *gambiae* melanotic capsules-associate proteome prior and following acid-treatment. Illustration
573 depicts that on each experimental condition (pre-acid and post-acid treatment), number of
574 identified proteins were found enriched in infected versus naïve midguts. **B,** Subset of *A. gambiae*
575 melanotic capsules-associated proteins ($N = 14$) demonstrating acid-resistance and enrichment in
576 *P. berghei* infected-midguts. Data represent proteins consistently identified across 2-5 biological

bioRxiv preprint doi: https://doi.org/10.1101/2021.05.07.443077; this version posted May 8, 2021. The copyright holder for this preprint (which was not certified by peer review) is the author/funder, who has granted bioRxiv a license to display the preprint in perpetuity. It is made available under aCC-BY 4.0 International license.

577 replicates (95% Peptide Threshold, 2 Peptides minimum, 95% Protein Threshold, 1 % FDR. Heat
578 map shows averaged normalized total spectra for each sample group. Control corresponds to
579 midguts from naïve blood-fed mosquitoes.
580
581 **Figure 3. AgMesh (AGAP000550) is highly conserved among main malaria and arboviral**
582 **vector mosquitoes.** *In silico* analyses of *A. gambiae* AGAP000550. **A,** Percentage identity
583 between amino acid sequences from main anopheline vectors of human malaria and major
584 arboviral vector mosquitoes. **B,** Comparison of the predicted domain structures of *A. gambiae*
585 AGAP000550 and its anopheline orthologue proteins: *A. albimanus* AALB006494, *A. stephensi*
586 ASTE001216, *A. arabiensis* AARA010496, and *A. dirus* ADIR001323. NIDO, extracellular
587 domain of unknown function. AMOP, adhesion-associated domain that occurs in putative cell
588 adhesion molecules. VWD, von Willebrand factor type D domain mediates interaction with blood
589 clotting factor VIII. SUSHI (CCP) complement control protein module containing four invariant
590 cysteine residues forming two disulfide-bridges involved in recognition processes.
591
592 **Figure 4. Effect of *Ag*Mesh RNAi-mediated gene silencing on *Plasmodium* infection in human**
593 **parasite and murine malaria models. A, Left,** Infection intensity and prevalence of human
594 malaria parasites *P. falciparum* in *Ag*Mesh-silenced *A. gambiae* (Keele strain) S mosquitoes. Each
595 circle indicates the number of oocysts on an individual midgut; horizontal bars represent the
596 median value of oocysts pooled from 3 independent experiments. Gene silencing efficiency: 23-
597 62%. **A, Right,** Rodent malaria parasites *P. berghei* infection intensity in *Ag*Mesh-silenced *A.*
598 *gambiae* (L3-5 strain) R mosquitoes. Gene silencing efficiency: ~70%. Live oocysts (L) and
599 melanized parasites (M) intensities were compared using the non-parametric Mann-Whitney test

bioRxiv preprint doi: https://doi.org/10.1101/2021.05.07.443077; this version posted May 8, 2021. The copyright holder for this preprint (which was not certified by peer review) is the author/funder, who has granted bioRxiv a license to display the preprint in perpetuity. It is made available under aCC-BY 4.0 International license.

600 (infection intensity). **B,** Prevalence of mosquito infection. Two-sided Fisher's exact test *P* value
601 was done to compared infection prevalence. **C,** Live and melanized parasites on individual
602 mosquito midguts. The medians from 2 independent experiments are indicated with red lines. Each
603 circle indicates the number of parasites on an individual midgut. dsGFP injected mosquitoes were
604 used as controls. **D,** Distribution of *P. berghei* parasite phenotypes in *Ag*Mesh-silenced *A. gambiae*
605 (L3-5 strain) R mosquitoes compared to control. Pie charts show the percentage of mosquito
606 midguts carrying live parasites only (red) and live and melanized parasites (gray).
607
608 **Figure S1.** Time-course isolation of *Anopheles* melanotic capsules during acid treatment and
609 heating at 80˚C. Light microscopy images at 20X, 40X, and 100X (oil immersion) prior and post
610 5-, 10-, 20-, 30-, 40-, 50-, and 60-min acid hydrolysis demonstrates acid-resistant and heat-stable
611 aggregated melanin-like material that tends to clump due to its hydrophobic nature. Bars 10 µm
612
613 **Figure S2**. Effect of *Ag*Mesh-silencing in the parasite's development 26 hpi in *A. gambiae* (L3-5
614 strain) R mosquitoes. **A,** Giemsa staining of lumen content of midgut to verifying presence of
615 several *Plasmodium* parasite immatures stages (red arrow heads) along with gut microbiota. **B,**
616 Confocal microscopy using anti-Pbs28 against *P. berghei* to detect parasite (white arrowhead)
617 invasion of the midgut epithelial cells.
618
619 **Table S1.** Subset of proteins from *Anopheles gambiae* (L3-5 strain) enriched in *Plasmodium*
620 *berghei*-infected midguts at 6 dpi (prior to acid treatment).
621

bioRxiv preprint doi: https://doi.org/10.1101/2021.05.07.443077; this version posted May 8, 2021. The copyright holder for this preprint (which was not certified by peer review) is the author/funder, who has granted bioRxiv a license to display the preprint in perpetuity. It is made available under aCC-BY 4.0 International license.

622 **Table S2.** Subset of acid-resistant midgut proteins from *Anopheles gambiae* (L3-5 strain)
623 identified associated to melanotic capsules against *Plasmodium berghei*.

624

625 **Table S3.** Primers used in this study.

626

627

628 **ACKNOWLEDGMENTS**

629 We would like to thank the Johns Hopkins Malaria Research Institute and Bloomberg
630 Philanthropies. We would like to acknowledge Barbara Smith for her expertise and technical
631 support with transmission EM and SEM at the Microscopy Facility, School of Medicine, Johns
632 Hopkins University. We also gratefully acknowledge Robert N. O'Meally for sample processing
633 and data acquisition related to proteomic analyses (Johns Hopkins Mass Spectrometry and
634 Proteomic Facility, The Johns Hopkins University). We thank Joel Tang for training on FTIR
635 acquisition and data analysis (Johns Hopkins NMR Core Facility, Department of Chemistry). The
636 following reagent was obtained through BEI Resources, NIAID, NIH: *Anopheles gambiae*, Strain
637 L35, MRA-114, deposited Mark Q. Benedict. EC, DFQS, and AC are funded by the Johns Hopkins
638 Malaria Research (JHMRI) Institute Pilot Grant Casadevall_123; EC, DFQS, and AC are funded
639 by NIAID R01 AI052733; EC was awardee of a Postdoctoral Fellowship from the Johns Hopkins
640 Malaria Research Institute. DFQS has been funded by NIH grants 5T32GM008752-18 and
641 1T32AI138953-01A1. GD, YD and YA were supported by the National Institutes of Health grants
642 R21AI131574, R01AI101431 and R01AI122743.

643

644

bioRxiv preprint doi: https://doi.org/10.1101/2021.05.07.443077; this version posted May 8, 2021. The copyright holder for this preprint (which was not certified by peer review) is the author/funder, who has granted bioRxiv a license to display the preprint in perpetuity. It is made available under aCC-BY 4.0 International license.

REFERENCES

1. Organization WH. World malaria report. Geneva, Switzerland: World Health Organization, 2018.

2. Medicine Io. Saving Lives, Buying Time: Economics of Malaria Drugs in an Age of Resistance. Arrow KJ, Panosian CB, Gelband H, editors. Washington, DC: The National Academies Press; 2004. 384 p.

3. Ghosh A, Edwards MJ, Jacobs-Lorena M. The journey of the malaria parasite in the mosquito: hopes for the new century. Parasitol Today. 2000;16(5):196-201. Epub 2000/04/27. doi: 10.1016/s0169-4758(99)01626-9. PubMed PMID: 10782078.

4. Dinglasan RR, Kalume DE, Kanzok SM, Ghosh AK, Muratova O, Pandey A, et al. Disruption of Plasmodium falciparum development by antibodies against a conserved mosquito midgut antigen. Proc Natl Acad Sci U S A. 2007;104(33):13461-6. Epub 2007/08/04. doi: 10.1073/pnas.0702239104. PubMed PMID: 17673553; PubMed Central PMCID: PMCPMC1948931.

5. Kotsyfakis M, Ehret-Sabatier L, Siden-Kiamos I, Mendoza J, Sinden RE, Louis C. Plasmodium berghei ookinetes bind to Anopheles gambiae and Drosophila melanogaster annexins. Mol Microbiol. 2005;57(1):171-9. Epub 2005/06/14. doi: 10.1111/j.1365-2958.2005.04664.x. PubMed PMID: 15948958.

6. Lavazec C, Bonnet S, Thiery I, Boisson B, Bourgouin C. cpbAg1 encodes an active carboxypeptidase B expressed in the midgut of Anopheles gambiae. Insect Mol Biol.

bioRxiv preprint doi: https://doi.org/10.1101/2021.05.07.443077; this version posted May 8, 2021. The copyright holder for this preprint (which was not certified by peer review) is the author/funder, who has granted bioRxiv a license to display the preprint in perpetuity. It is made available under aCC-BY 4.0 International license.

667 2005;14(2):163-74. Epub 2005/03/31. doi: 10.1111/j.1365-2583.2004.00541.x. PubMed PMID:
668 15796749.
669 7. Gonzalez-Lazaro M, Dinglasan RR, Hernandez-Hernandez Fde L, Rodriguez MH, Laclaustra
670 M, Jacobs-Lorena M, et al. Anopheles gambiae Croquemort SCRBQ2, expression profile in the
671 mosquito and its potential interaction with the malaria parasite Plasmodium berghei. Insect
672 Biochem Mol Biol. 2009;39(5-6):395-402. Epub 2009/04/16. doi: 10.1016/j.ibmb.2009.03.008.
673 PubMed PMID: 19366631; PubMed Central PMCID: PMCPMC4138513.
674 8. Vega-Rodriguez J, Ghosh AK, Kanzok SM, Dinglasan RR, Wang S, Bongio NJ, et al. Multiple
675 pathways for Plasmodium ookinete invasion of the mosquito midgut. Proc Natl Acad Sci U S A.
676 2014;111(4):E492-500. Epub 2014/01/30. doi: 10.1073/pnas.1315517111. PubMed PMID:
677 24474798; PubMed Central PMCID: PMCPMC3910608.
678 9. Sinden RE, Billingsley PF. Plasmodium invasion of mosquito cells: hawk or dove? Trends
679 Parasitol. 2001;17(5):209-12. Epub 2001/04/27. doi: 10.1016/s1471-4922(01)01928-6. PubMed
680 PMID: 11323288.
681 10. Alavi Y, Arai M, Mendoza J, Tufet-Bayona M, Sinha R, Fowler K, et al. The dynamics of
682 interactions between Plasmodium and the mosquito: a study of the infectivity of Plasmodium
683 berghei and Plasmodium gallinaceum, and their transmission by Anopheles stephensi, Anopheles
684 gambiae and Aedes aegypti. Int J Parasitol. 2003;33(9):933-43. Epub 2003/08/09. doi:
685 10.1016/s0020-7519(03)00112-7. PubMed PMID: 12906877.
686 11. Schwartz A, Koella JC. Melanization of plasmodium falciparum and C-25 sephadex beads
687 by field-caught Anopheles gambiae (Diptera: Culicidae) from southern Tanzania. J Med Entomol.
688 2002;39(1):84-8. Epub 2002/04/05. doi: 10.1603/0022-2585-39.1.84. PubMed PMID: 11931276.

bioRxiv preprint doi: https://doi.org/10.1101/2021.05.07.443077; this version posted May 8, 2021. The copyright holder for this preprint (which was not certified by peer review) is the author/funder, who has granted bioRxiv a license to display the preprint in perpetuity. It is made available under aCC-BY 4.0 International license.

12. Ramphul UN, Garver LS, Molina-Cruz A, Canepa GE, Barillas-Mury C. Plasmodium falciparum evades mosquito immunity by disrupting JNK-mediated apoptosis of invaded midgut cells. Proc Natl Acad Sci U S A. 2015;112(5):1273-80. Epub 2015/01/02. doi: 10.1073/pnas.1423586112. PubMed PMID: 25552553; PubMed Central PMCID: PMCPMC4321252.

13. Molina-Cruz A, DeJong RJ, Ortega C, Haile A, Abban E, Rodrigues J, et al. Some strains of Plasmodium falciparum, a human malaria parasite, evade the complement-like system of Anopheles gambiae mosquitoes. Proc Natl Acad Sci U S A. 2012;109(28):E1957-62. Epub 2012/05/25. doi: 10.1073/pnas.1121183109. PubMed PMID: 22623529; PubMed Central PMCID: PMCPMC3396512.

14. Lambrechts L, Morlais I, Awono-Ambene PH, Cohuet A, Simard F, Jacques JC, et al. Effect of infection by Plasmodium falciparum on the melanization immune response of Anopheles gambiae. Am J Trop Med Hyg. 2007;76(3):475-80. Epub 2007/03/16. PubMed PMID: 17360870.

15. d'Ischia M, Napolitano A, Pezzella A, Meredith P, Buehler M. Melanin Biopolymers: Tailoring Chemical Complexity for Materials Design. Angew Chem Int Ed Engl. 2019. Epub 2019/12/24. doi: 10.1002/anie.201914276. PubMed PMID: 31867862.

16. Sugumaran M, Barek H. Critical Analysis of the Melanogenic Pathway in Insects and Higher Animals. Int J Mol Sci. 2016;17(10). doi: 10.3390/ijms17101753. PubMed PMID: 27775611; PubMed Central PMCID: PMCPMC5085778.

17. Hillyer JF. Insect immunology and hematopoiesis. Dev Comp Immunol. 2016;58:102-18. doi: 10.1016/j.dci.2015.12.006. PubMed PMID: 26695127; PubMed Central PMCID: PMCPMC4775421.

bioRxiv preprint doi: https://doi.org/10.1101/2021.05.07.443077; this version posted May 8, 2021. The copyright holder for this preprint (which was not certified by peer review) is the author/funder, who has granted bioRxiv a license to display the preprint in perpetuity. It is made available under aCC-BY 4.0 International license.

711 18. Whitten MMA, Coates CJ. Re-evaluation of insect melanogenesis research: Views from
712 the dark side. Pigment Cell Melanoma Res. 2017;30(4):386-401. Epub 2017/04/06. doi:
713 10.1111/pcmr.12590. PubMed PMID: 28378380.
714 19. Camacho E, Vij R, Chrissian C, Prados-Rosales R, Gil D, O'Meally RN, et al. The structural
715 unit of melanin in the cell wall of the fungal pathogen Cryptococcus neoformans. J Biol Chem.
716 2019;294(27):10471-89. Epub 2019/05/24. doi: 10.1074/jbc.RA119.008684. PubMed PMID:
717 31118223; PubMed Central PMCID: PMCPMC6615676.
718 20. Eisenman HC, Frases S, Nicola AM, Rodrigues ML, Casadevall A. Vesicle-associated
719 melanization in Cryptococcus neoformans. Microbiology. 2009;155(Pt 12):3860-7. Epub
720 2009/09/05. doi: 10.1099/mic.0.032854-0. PubMed PMID: 19729402; PubMed Central PMCID:
721 PMCPMC2889422.
722 21. C. D, F. G, S. MM, G. R. Biogenesis of Melanosomes. In: Jan B, P.A R, editors. Melanins and
723 Melanosomes: Biosynthesis, Biogenesis, Physiological, and Pathological Functions. 1rst ed. Wiley-
724 VCH Verlag GmbH & Co. KGaA Weinheim, Germany; 2011. p. 247-94.
725 22. Falabella P, Riviello L, Pascale M, Lelio ID, Tettamanti G, Grimaldi A, et al. Functional
726 amyloids in insect immune response. Insect Biochem Mol Biol. 2012;42(3):203-11. Epub
727 2011/12/31. doi: 10.1016/j.ibmb.2011.11.011. PubMed PMID: 22207151.
728 23. Grimaldi A, Tettamanti G, Congiu T, Girardello R, Malagoli D, Falabella P, et al. The main
729 actors involved in parasitization of Heliothis virescens larva. Cell Tissue Res. 2012;350(3):491-
730 502. Epub 2012/10/12. doi: 10.1007/s00441-012-1503-8. PubMed PMID: 23053052.
731 24. Clark KD. Insect Hemolymph Immune Complexes. Subcell Biochem. 2020;94:123-61. Epub
732 2020/03/20. doi: 10.1007/978-3-030-41769-7_5. PubMed PMID: 32189298.

bioRxiv preprint doi: https://doi.org/10.1101/2021.05.07.443077; this version posted May 8, 2021. The copyright holder for this preprint (which was not certified by peer review) is the author/funder, who has granted bioRxiv a license to display the preprint in perpetuity. It is made available under aCC-BY 4.0 International license.

733 25. Blandin S, Levashina EA. Mosquito immune responses against malaria parasites. Current
734 Opinion in Immunology. 2004;16(1):16-20. doi: 10.1016/j.coi.2003.11.010.
735 26. El Moussawi L, Nakhleh J, Kamareddine L, Osta MA. The mosquito melanization response
736 requires hierarchical activation of non-catalytic clip domain serine protease homologs. PLoS
737 Pathog. 2019;15(11):e1008194. Epub 2019/11/26. doi: 10.1371/journal.ppat.1008194. PubMed
738 PMID: 31765430; PubMed Central PMCID: PMCPMC6901238.
739 27. Yan Y, Hillyer JF. Complement-like proteins TEP1, TEP3 and TEP4 are positive regulators
740 of periostial hemocyte aggregation in the mosquito Anopheles gambiae. Insect Biochem Mol Biol.
741 2019;107:1-9. Epub 2019/01/29. doi: 10.1016/j.ibmb.2019.01.007. PubMed PMID: 30690067.
742 28. Di Lelio I, Varricchio P, Di Prisco G, Marinelli A, Lasco V, Caccia S, et al. Functional analysis
743 of an immune gene of Spodoptera littoralis by RNAi. J Insect Physiol. 2014;64:90-7. Epub
744 2014/03/26. doi: 10.1016/j.jinsphys.2014.03.008. PubMed PMID: 24662467.
745 29. Chatterjee S, Prados-Rosales R, Itin B, Casadevall A, Stark RE. Solid-state NMR Reveals the
746 Carbon-based Molecular Architecture of Cryptococcus neoformans Fungal Eumelanins in the Cell
747 Wall. J Biol Chem. 2015;290(22):13779-90. Epub 2015/04/01. doi: 10.1074/jbc.M114.618389.
748 PubMed PMID: 25825492; PubMed Central PMCID: PMCPMC4447955.
749 30. Camacho E, Chrissian C, Cordero RJB, Liporagi-Lopes L, Stark RE, Casadevall A. N-
750 acetylglucosamine affects Cryptococcus neoformans cell-wall composition and melanin
751 architecture. Microbiology. 2017;163(11):1540-56. Epub 2017/10/19. doi:
752 10.1099/mic.0.000552. PubMed PMID: 29043954; PubMed Central PMCID: PMCPMC5775898.
753 31. Chrissian C, Camacho E, Fu MS, Prados-Rosales R, Chatterjee S, Cordero RJB, et al. Melanin
754 deposition in two Cryptococcus species depends on cell-wall composition and flexibility. J Biol

bioRxiv preprint doi: https://doi.org/10.1101/2021.05.07.443077; this version posted May 8, 2021. The copyright holder for this preprint (which was not certified by peer review) is the author/funder, who has granted bioRxiv a license to display the preprint in perpetuity. It is made available under aCC-BY 4.0 International license.

Chem. 2020;295(7):1815-28. Epub 2020/01/04. doi: 10.1074/jbc.RA119.011949. PubMed PMID: 31896575.

32. Collins FH, Sakai RK, Vernick KD, Paskewitz S, Seeley DC, Miller LH, et al. Genetic selection of a Plasmodium-refractory strain of the malaria vector Anopheles gambiae. Science. 1986;234(4776):607-10. Epub 1986/10/31. doi: 10.1126/science.3532325. PubMed PMID: 3532325.

33. Goncalves RL, Oliveira JH, Oliveira GA, Andersen JF, Oliveira MF, Oliveira PL, et al. Mitochondrial reactive oxygen species modulate mosquito susceptibility to Plasmodium infection. PLoS One. 2012;7(7):e41083. Epub 2012/07/21. doi: 10.1371/journal.pone.0041083. PubMed PMID: 22815925; PubMed Central PMCID: PMCPMC3399787.

34. Rosas AL, Nosanchuk JD, Gomez BL, Edens WA, Henson JM, Casadevall A. Isolation and serological analyses of fungal melanins. J Immunol Methods. 2000;244(1-2):69-80. PubMed PMID: 11033020.

35. Nosanchuk JD, Stark RE, Casadevall A. Fungal Melanin: What do We Know About Structure? Front Microbiol. 2015;6:1463. Epub 2016/01/07. doi: 10.3389/fmicb.2015.01463. PubMed PMID: 26733993; PubMed Central PMCID: PMCPMC4687393.

36. Camacho E, Vij R, Chrissian C, Prados-Rosales R, Gil D, O'Meally RN, et al. The structural unit of melanin in the cell wall of the fungal pathogen Cryptococcus neoformans. J Biol Chem. 2019. doi: 10.1074/jbc.RA119.008684. PubMed PMID: 31118223.

37. Meredith P, Sarna T. The physical and chemical properties of eumelanin. Pigment Cell Res. 2006;19(6):572-94. doi: 10.1111/j.1600-0749.2006.00345.x. PubMed PMID: 17083485.

bioRxiv preprint doi: https://doi.org/10.1101/2021.05.07.443077; this version posted May 8, 2021. The copyright holder for this preprint (which was not certified by peer review) is the author/funder, who has granted bioRxiv a license to display the preprint in perpetuity. It is made available under aCC-BY 4.0 International license.

776 38. Al Khatib M, Harir M, Costa J, Baratto MC, Schiavo I, Trabalzini L, et al. Spectroscopic
777 Characterization of Natural Melanin from a Streptomyces cyaneofuscatus Strain and Comparison
778 with Melanin Enzymatically Synthesized by Tyrosinase and Laccase. Molecules. 2018;23(8). Epub
779 2018/08/04. doi: 10.3390/molecules23081916. PubMed PMID: 30071605; PubMed Central
780 PMCID: PMCPMC6222888.
781 39. Zhang M, Xiao G, Thring RW, Chen W, Zhou H, Yang H. Production and Characterization
782 of Melanin by Submerged Culture of Culinary and Medicinal Fungi Auricularia auricula. Appl
783 Biochem Biotechnol. 2015;176(1):253-66. Epub 2015/03/25. doi: 10.1007/s12010-015-1571-9.
784 PubMed PMID: 25800528.
785 40. Li C, Ji C, Tang B. Purification, characterisation and biological activity of melanin from
786 Streptomyces sp. FEMS Microbiol Lett. 2018;365(19). Epub 2018/06/19. doi:
787 10.1093/femsle/fny077. PubMed PMID: 29912354.
788 41. De Souza RA, Kamat NM, Nadkarni VS. Purification and characterisation of a sulphur rich
789 melanin from edible mushroom Termitomyces albuminosus Heim. Mycology. 2018;9(4):296-306.
790 Epub 2018/12/12. doi: 10.1080/21501203.2018.1494060. PubMed PMID: 30533254; PubMed
791 Central PMCID: PMCPMC6282441.
792 42. Padron A, Molina-Cruz A, Quinones M, Ribeiro JM, Ramphul U, Rodrigues J, et al. In depth
793 annotation of the Anopheles gambiae mosquito midgut transcriptome. BMC Genomics.
794 2014;15:636. Epub 2014/07/31. doi: 10.1186/1471-2164-15-636. PubMed PMID: 25073905;
795 PubMed Central PMCID: PMCPMC4131051.
796 43. Parish LA, Colquhoun DR, Ubaida Mohien C, Lyashkov AE, Graham DR, Dinglasan RR.
797 Ookinete-interacting proteins on the microvillar surface are partitioned into detergent resistant

bioRxiv preprint doi: https://doi.org/10.1101/2021.05.07.443077; this version posted May 8, 2021. The copyright holder for this preprint (which was not certified by peer review) is the author/funder, who has granted bioRxiv a license to display the preprint in perpetuity. It is made available under aCC-BY 4.0 International license.

membranes of Anopheles gambiae midguts. J Proteome Res. 2011;10(11):5150-62. doi: 10.1021/pr2006268. PubMed PMID: 21905706; PubMed Central PMCID: PMCPMC3208356.

44. Dinglasan RR, Devenport M, Florens L, Johnson JR, McHugh CA, Donnelly-Doman M, et al. The Anopheles gambiae adult midgut peritrophic matrix proteome. Insect Biochem Mol Biol. 2009;39(2):125-34. Epub 2008/11/29. doi: 10.1016/j.ibmb.2008.10.010. PubMed PMID: 19038338; PubMed Central PMCID: PMCPMC2684889.

45. Izumi Y, Yanagihashi Y, Furuse M. A novel protein complex, Mesh-Ssk, is required for septate junction formation in the Drosophila midgut. J Cell Sci. 2012;125(Pt 20):4923-33. doi: 10.1242/jcs.112243. PubMed PMID: 22854041.

46. Simonetti AB, Billingsley PF, Winger LA, Sinden RE. Kinetics of expression of two major Plasmodium berghei antigens in the mosquito vector, Anopheles stephensi. J Eukaryot Microbiol. 1993;40(5):569-76. Epub 1993/09/01. doi: 10.1111/j.1550-7408.1993.tb06109.x. PubMed PMID: 8401470.

47. Prota G. Progress in the chemistry of melanins and related metabolites. Med Res Rev. 1988;8(4):525-56. Epub 1988/10/01. doi: 10.1002/med.2610080405. PubMed PMID: 3057299.

48. Barek H, Sugumaran M, Ito S, Wakamatsu K. Insect cuticular melanins are distinctly different from those of mammalian epidermal melanins. Pigment Cell Melanoma Res. 2018;31(3):384-92. Epub 2017/11/22. doi: 10.1111/pcmr.12672. PubMed PMID: 29160957.

49. Galvan I, Jorge A, Edelaar P, Wakamatsu K. Insects synthesize pheomelanin. Pigment Cell Melanoma Res. 2015;28(5):599-602. doi: 10.1111/pcmr.12397. PubMed PMID: 26176957.

bioRxiv preprint doi: https://doi.org/10.1101/2021.05.07.443077; this version posted May 8, 2021. The copyright holder for this preprint (which was not certified by peer review) is the author/funder, who has granted bioRxiv a license to display the preprint in perpetuity. It is made available under aCC-BY 4.0 International license.

818 50. Polidori C, Jorge A, Ornosa C. Eumelanin and pheomelanin are predominant pigments in
819 bumblebee (Apidae: Bombus) pubescence. PeerJ. 2017;5:e3300. Epub 2017/06/01. doi:
820 10.7717/peerj.3300. PubMed PMID: 28560094; PubMed Central PMCID: PMCPMC5445944.
821 51. Jorge Garcia A, Polidori C, Nieves-Aldrey JL. Pheomelanin in the secondary sexual
822 characters of male parasitoid wasps (Hymenoptera: Pteromalidae). Arthropod Struct Dev.
823 2016;45(4):311-9. Epub 2016/05/26. doi: 10.1016/j.asd.2016.05.001. PubMed PMID: 27224206.
824 52. Ito S, Wakamatsu K. Chemistry of mixed melanogenesis--pivotal roles of dopaquinone.
825 Photochem Photobiol. 2008;84(3):582-92. Epub 2008/04/26. doi: 10.1111/j.1751-
826 1097.2007.00238.x. PubMed PMID: 18435614.
827 53. Engelen M, Vanna R, Bellei C, Zucca FA, Wakamatsu K, Monzani E, et al. Neuromelanins
828 of human brain have soluble and insoluble components with dolichols attached to the melanic
829 structure. PLoS One. 2012;7(11):e48490. Epub 2012/11/10. doi: 10.1371/journal.pone.0048490.
830 PubMed PMID: 23139786; PubMed Central PMCID: PMCPMC3489676.
831 54. Dubey S, Roulin A. Evolutionary and biomedical consequences of internal melanins.
832 Pigment Cell Melanoma Res. 2014;27(3):327-38. Epub 2014/05/21. doi: 10.1111/pcmr.12231.
833 PubMed PMID: 24843888.
834 55. Dong Y, Aguilar R, Xi Z, Warr E, Mongin E, Dimopoulos G. Anopheles gambiae Immune
835 Responses to Human and Rodent Plasmodium Parasite Species. PLoS Pathogens. 2006;2(6):e52.
836 doi: 10.1371/journal.ppat.0020052.
837 56. Blandin S, Shiao SH, Moita LF, Janse CJ, Waters AP, Kafatos FC, et al. Complement-like
838 protein TEP1 is a determinant of vectorial capacity in the malaria vector Anopheles gambiae. Cell.

bioRxiv preprint doi: https://doi.org/10.1101/2021.05.07.443077; this version posted May 8, 2021. The copyright holder for this preprint (which was not certified by peer review) is the author/funder, who has granted bioRxiv a license to display the preprint in perpetuity. It is made available under aCC-BY 4.0 International license.

2004;116(5):661-70. Epub 2004/03/10. doi: 10.1016/s0092-8674(04)00173-4. PubMed PMID: 15006349.

57. Dong Y, Manfredini F, Dimopoulos G. Implication of the mosquito midgut microbiota in the defense against malaria parasites. PLoS Pathog. 2009;5(5):e1000423. Epub 2009/05/09. doi: 10.1371/journal.ppat.1000423. PubMed PMID: 19424427; PubMed Central PMCID: PMCPMC2673032.

58. Kumar S, Christophides GK, Cantera R, Charles B, Han YS, Meister S, et al. The role of reactive oxygen species on Plasmodium melanotic encapsulation in Anopheles gambiae. Proc Natl Acad Sci U S A. 2003;100(24):14139-44. doi: 10.1073/pnas.2036262100. PubMed PMID: 14623973; PubMed Central PMCID: PMCPMC283559.

59. Oliveira JH, Goncalves RL, Oliveira GA, Oliveira PL, Oliveira MF, Barillas-Mury C. Energy metabolism affects susceptibility of Anopheles gambiae mosquitoes to Plasmodium infection. Insect Biochem Mol Biol. 2011;41(6):349-55. Epub 2011/02/16. doi: 10.1016/j.ibmb.2011.02.001. PubMed PMID: 21320598; PubMed Central PMCID: PMCPMC3078167.

60. Trisnadi N, Barillas-Mury C. Live In Vivo Imaging of Plasmodium Invasion of the Mosquito Midgut. mSphere. 2020;5(5). Epub 2020/09/04. doi: 10.1128/mSphere.00692-20. PubMed PMID: 32878934; PubMed Central PMCID: PMCPMC7471008.

61. Han YS, Thompson J, Kafatos FC, Barillas-Mury C. Molecular interactions between Anopheles stephensi midgut cells and Plasmodium berghei: the time bomb theory of ookinete invasion of mosquitoes. EMBO J. 2000;19(22):6030-40. Epub 2000/11/18. doi:

bioRxiv preprint doi: https://doi.org/10.1101/2021.05.07.443077; this version posted May 8, 2021. The copyright holder for this preprint (which was not certified by peer review) is the author/funder, who has granted bioRxiv a license to display the preprint in perpetuity. It is made available under aCC-BY 4.0 International license.

10.1093/emboj/19.22.6030. PubMed PMID: 11080150; PubMed Central PMCID: PMCPMC305834.

62. Shandala T, Woodcock JM, Ng Y, Biggs L, Skoulakis EM, Brooks DA, et al. Drosophila 14-3-3epsilon has a crucial role in anti-microbial peptide secretion and innate immunity. J Cell Sci. 2011;124(Pt 13):2165-74. Epub 2011/06/15. doi: 10.1242/jcs.080598. PubMed PMID: 21670199.

63. Trujillo-Ocampo A, Cazares-Raga FE, Del Angel RM, Medina-Ramirez F, Santos-Argumedo L, Rodriguez MH, et al. Participation of 14-3-3epsilon and 14-3-3zeta proteins in the phagocytosis, component of cellular immune response, in Aedes mosquito cell lines. Parasit Vectors. 2017;10(1):362. Epub 2017/08/03. doi: 10.1186/s13071-017-2267-5. PubMed PMID: 28764795; PubMed Central PMCID: PMCPMC5540338.

64. Simões ML, Mlambo G, Mlambo G, Tripathi A, Dong Y, George D. Immune Regulation of Plasmodium Is Anopheles Species Specific and Infection Intensity Dependent. MBio. 2017;8(5):e01631-17. doi: https://doi.org/10.1128/.

65. Paskewitz SM, Brown MR, Lea AO, Collins FH. Ultrastructure of the encapsulation of Plasmodium cynomolgi (B strain) on the midgut of a refractory strain of Anopheles gambiae. J Parasitol. 1988;74(3):432-9. Epub 1988/06/01. PubMed PMID: 3379524.

66. Ubaida Mohien C, Colquhoun DR, Mathias DK, Gibbons JG, Armistead JS, Rodriguez MC, et al. A bioinformatics approach for integrated transcriptomic and proteomic comparative analyses of model and non-sequenced anopheline vectors of human malaria parasites. Mol Cell Proteomics. 2013;12(1):120-31. Epub 2012/10/20. doi: 10.1074/mcp.M112.019596. PubMed PMID: 23082028; PubMed Central PMCID: PMCPMC3536893.

bioRxiv preprint doi: https://doi.org/10.1101/2021.05.07.443077; this version posted May 8, 2021. The copyright holder for this preprint (which was not certified by peer review) is the author/funder, who has granted bioRxiv a license to display the preprint in perpetuity. It is made available under aCC-BY 4.0 International license.

881 67. Jorieux S, Fressinaud E, Goudemand J, Gaucher C, Meyer D, Mazurier C. Conformational
882 changes in the D' domain of von Willebrand factor induced by CYS 25 and CYS 95 mutations lead
883 to factor VIII binding defect and multimeric impairment. Blood. 2000;95(10):3139-45. Epub
884 2000/05/16. PubMed PMID: 10807780.
885 68. Voorberg J, Fontijn R, van Mourik JA, Pannekoek H. Domains involved in multimer
886 assembly of von willebrand factor (vWF): multimerization is independent of dimerization. EMBO
887 J. 1990;9(3):797-803. Epub 1990/03/01. PubMed PMID: 2311582; PubMed Central PMCID:
888 PMCPMC551739.
889 69. Waterhouse RM, Kriventseva EV, Meister S, Xi Z, Alvarez KS, Bartholomay LC, et al.
890 Evolutionary dynamics of immune-related genes and pathways in disease-vector mosquitoes.
891 Science. 2007;316(5832):1738-43. Epub 2007/06/26. doi: 10.1126/science.1139862. PubMed
892 PMID: 17588928; PubMed Central PMCID: PMCPMC2042107.
893 70. Oliveira JH, Goncalves RL, Lara FA, Dias FA, Gandara AC, Menna-Barreto RF, et al. Blood
894 meal-derived heme decreases ROS levels in the midgut of Aedes aegypti and allows proliferation
895 of intestinal microbiota. PLoS Pathog. 2011;7(3):e1001320. Epub 2011/03/30. doi:
896 10.1371/journal.ppat.1001320. PubMed PMID: 21445237; PubMed Central PMCID:
897 PMCPMC3060171.
898 71. Kumar S, Molina-Cruz A, Gupta L, Rodrigues J, Barillas-Mury C. A peroxidase/dual oxidase
899 system modulates midgut epithelial immunity in Anopheles gambiae. Science.
900 2010;327(5973):1644-8. Epub 2010/03/13. doi: 10.1126/science.1184008. PubMed PMID:
901 20223948; PubMed Central PMCID: PMCPMC3510679.

bioRxiv preprint doi: https://doi.org/10.1101/2021.05.07.443077; this version posted May 8, 2021. The copyright holder for this preprint (which was not certified by peer review) is the author/funder, who has granted bioRxiv a license to display the preprint in perpetuity. It is made available under aCC-BY 4.0 International license.

902 72. Xiao X, Yang L, Pang X, Zhang R, Zhu Y, Wang P, et al. A Mesh-Duox pathway regulates
903 homeostasis in the insect gut. Nat Microbiol. 2017;2:17020. Epub 2017/03/02. doi:
904 10.1038/nmicrobiol.2017.20. PubMed PMID: 28248301; PubMed Central PMCID:
905 PMCPMC5332881.
906 73. Ha EM, Lee KA, Seo YY, Kim SH, Lim JH, Oh BH, et al. Coordination of multiple dual oxidase-
907 regulatory pathways in responses to commensal and infectious microbes in drosophila gut. Nat
908 Immunol. 2009;10(9):949-57. Epub 2009/08/12. doi: 10.1038/ni.1765. PubMed PMID: 19668222.
909 74. Jang S, Mergaert P, Ohbayashi T, Ishigami K, Shigenobu S, Itoh H, et al. Dual oxidase
910 enables insect gut symbiosis by mediating respiratory network formation. Proc Natl Acad Sci U S
911 A. 2021;118(10). Epub 2021/03/03. doi: 10.1073/pnas.2020922118. PubMed PMID: 33649233.
912 75. Yang X, Smith AA, Williams MS, Pal U. A dityrosine network mediated by dual oxidase and
913 peroxidase influences the persistence of Lyme disease pathogens within the vector. J Biol Chem.
914 2014;289(18):12813-22. Epub 2014/03/26. doi: 10.1074/jbc.M113.538272. PubMed PMID:
915 24662290; PubMed Central PMCID: PMCPMC4007469.
916 76. Jaramillo-Gutierrez G, Molina-Cruz A, Kumar S, Barillas-Mury C. The Anopheles gambiae
917 oxidation resistance 1 (OXR1) gene regulates expression of enzymes that detoxify reactive oxygen
918 species. PLoS One. 2010;5(6):e11168. Epub 2010/06/23. doi: 10.1371/journal.pone.0011168.
919 PubMed PMID: 20567517; PubMed Central PMCID: PMCPMC2887368.
920 77. Rodgers FH, Gendrin M, Wyer CAS, Christophides GK. Microbiota-induced peritrophic
921 matrix regulates midgut homeostasis and prevents systemic infection of malaria vector
922 mosquitoes. PLoS Pathog. 2017;13(5):e1006391. Epub 2017/05/26. doi:

bioRxiv preprint doi: https://doi.org/10.1101/2021.05.07.443077; this version posted May 8, 2021. The copyright holder for this preprint (which was not certified by peer review) is the author/funder, who has granted bioRxiv a license to display the preprint in perpetuity. It is made available under aCC-BY 4.0 International license.

923 10.1371/journal.ppat.1006391. PubMed PMID: 28545061; PubMed Central PMCID:
924 PMCPMC5448818.
925 78. Kuraishi T, Binggeli O, Opota O, Buchon N, Lemaitre B. Genetic evidence for a protective
926 role of the peritrophic matrix against intestinal bacterial infection in Drosophila melanogaster.
927 Proc Natl Acad Sci U S A. 2011;108(38):15966-71. Epub 2011/09/08. doi:
928 10.1073/pnas.1105994108. PubMed PMID: 21896728; PubMed Central PMCID:
929 PMCPMC3179054.
930 79. Ciccarelli FD, Doerks T, Bork P. AMOP, a protein module alternatively spliced in cancer
931 cells. Trends Biochem Sci. 2002;27(3):113-5. Epub 2002/03/15. doi: 10.1016/s0968-
932 0004(01)02049-7. PubMed PMID: 11893501.
933 80. Perez-Vilar J, Hill RL. The structure and assembly of secreted mucins. J Biol Chem.
934 1999;274(45):31751-4. Epub 1999/11/05. doi: 10.1074/jbc.274.45.31751. PubMed PMID:
935 10542193.
936 81. Chrissian C, Lin CP, Camacho E, Casadevall A, Neiman AM, Stark RE. Unconventional
937 Constituents and Shared Molecular Architecture of the Melanized Cell Wall of C. neoformans and
938 Spore Wall of S. cerevisiae. J Fungi (Basel). 2020;6(4). Epub 2020/12/05. doi:
939 10.3390/jof6040329. PubMed PMID: 33271921; PubMed Central PMCID: PMCPMC7712904.
940 82. Keller A, Nesvizhskii AI, Kolker E, Aebersold R. Empirical statistical model to estimate the
941 accuracy of peptide identifications made by MS/MS and database search. Anal Chem.
942 2002;74(20):5383-92. Epub 2002/10/31. doi: 10.1021/ac025747h. PubMed PMID: 12403597.

bioRxiv preprint doi: https://doi.org/10.1101/2021.05.07.443077; this version posted May 8, 2021. The copyright holder for this preprint (which was not certified by peer review) is the author/funder, who has granted bioRxiv a license to display the preprint in perpetuity. It is made available under aCC-BY 4.0 International license.

943 83. Hulo N, Bairoch A, Bulliard V, Cerutti L, Cuche BA, de Castro E, et al. The 20 years of
944 PROSITE. Nucleic Acids Res. 2008;36(Database issue):D245-9. Epub 2007/11/16. doi:
945 10.1093/nar/gkm977. PubMed PMID: 18003654; PubMed Central PMCID: PMCPMC2238851.

946

947

948

949

950

bioRxiv preprint doi: https://doi.org/10.1101/2021.05.07.443077; this version posted May 8, 2021. The copyright holder for this preprint (which was not certified by peer review) is the author/funder, who has granted bioRxiv a license to display the preprint in perpetuity. It is made available under aCC-BY 4.0 International license.

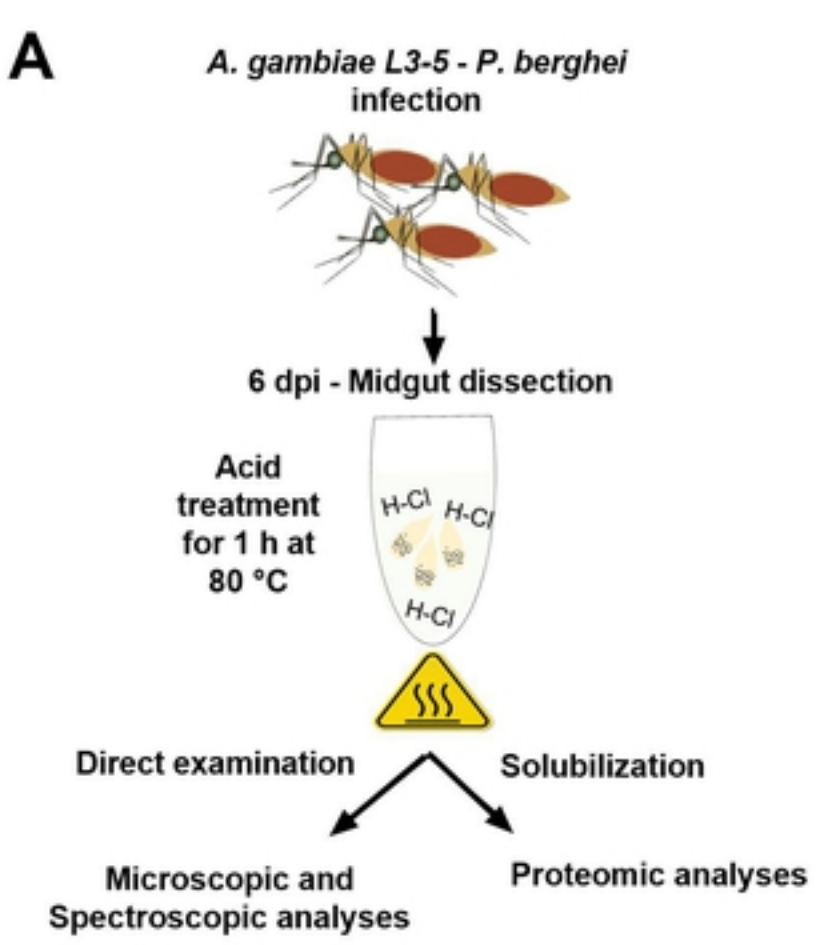

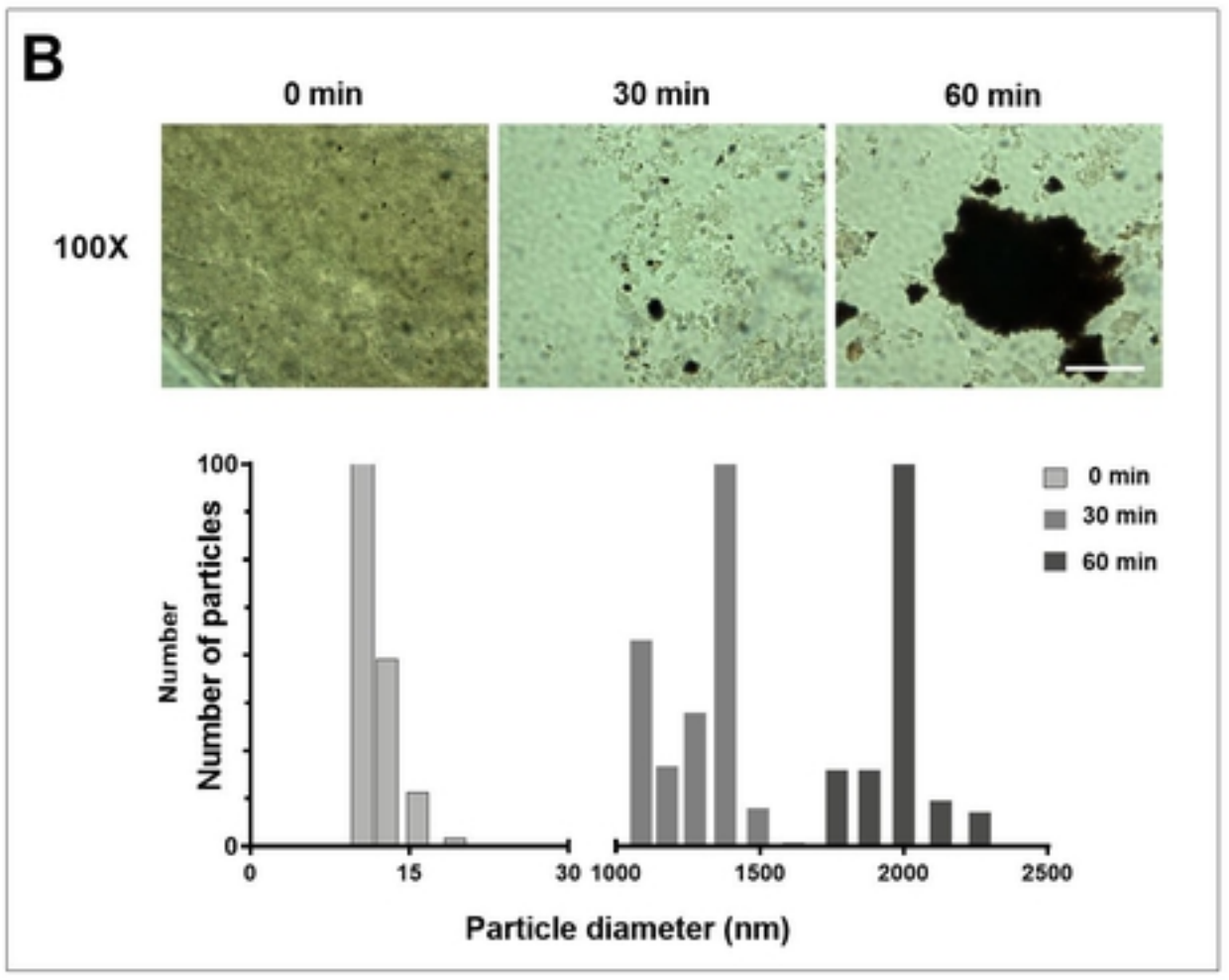

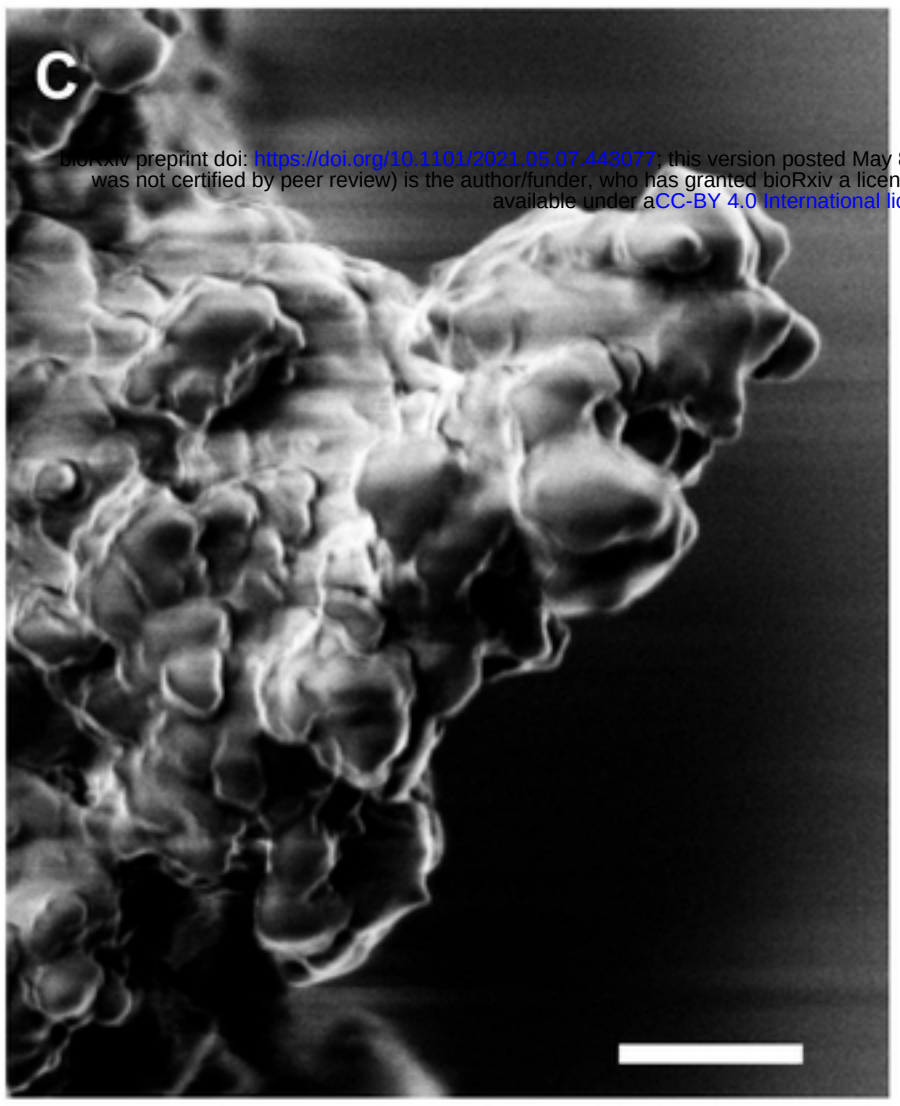

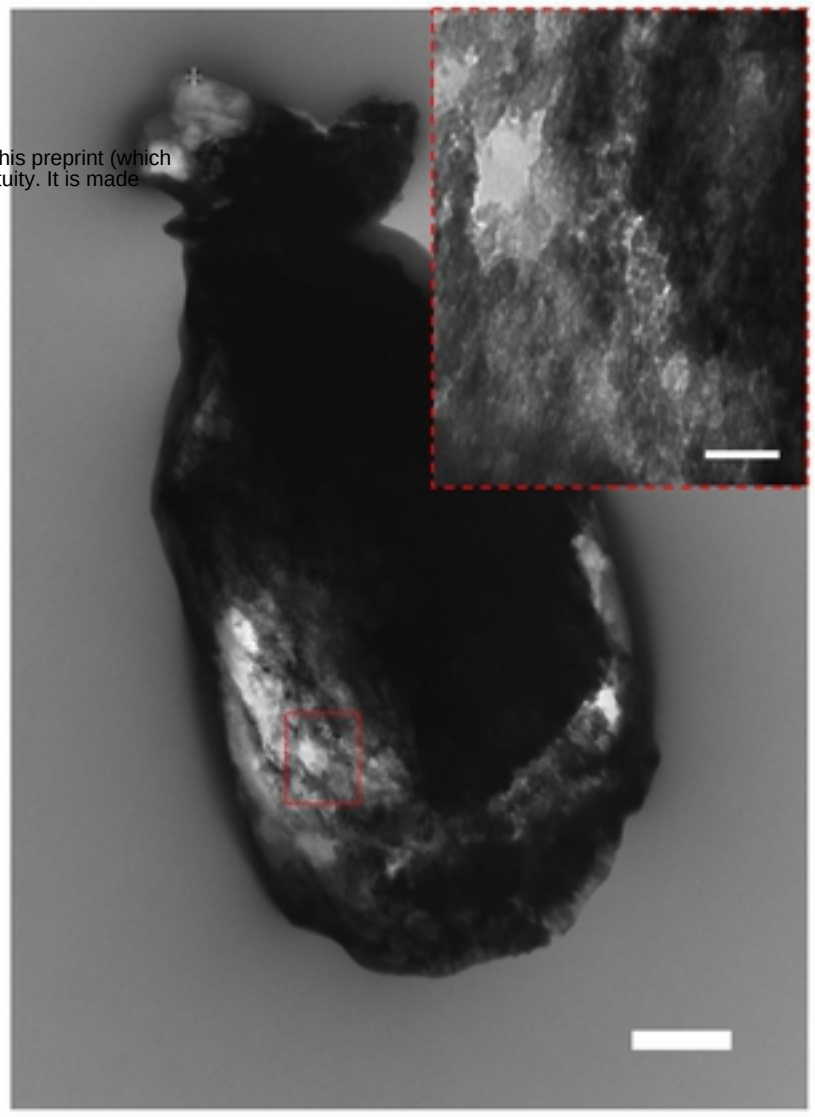

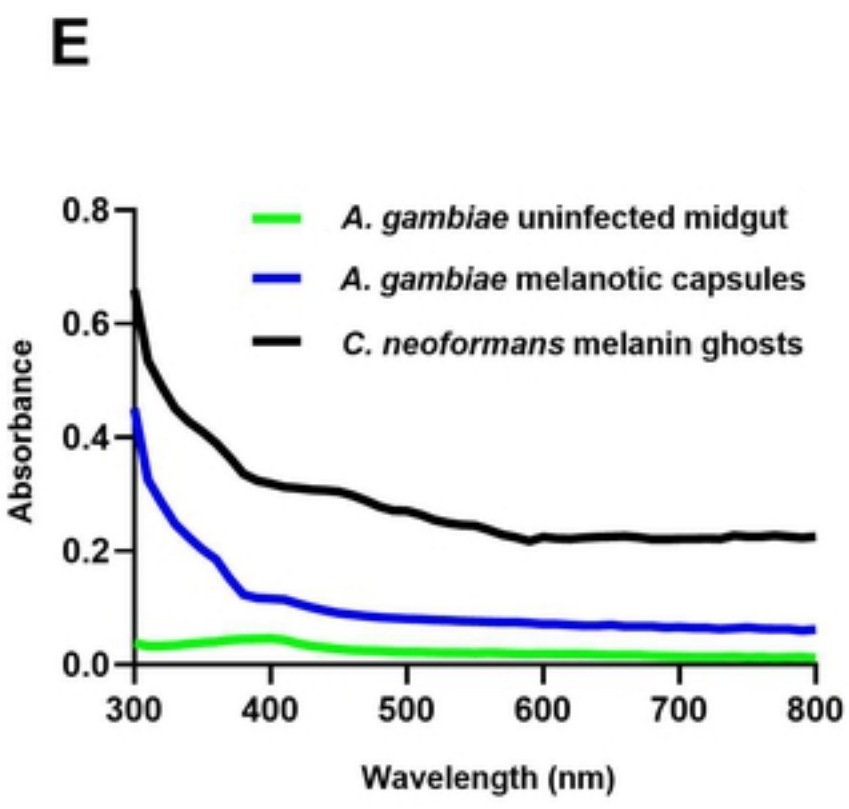

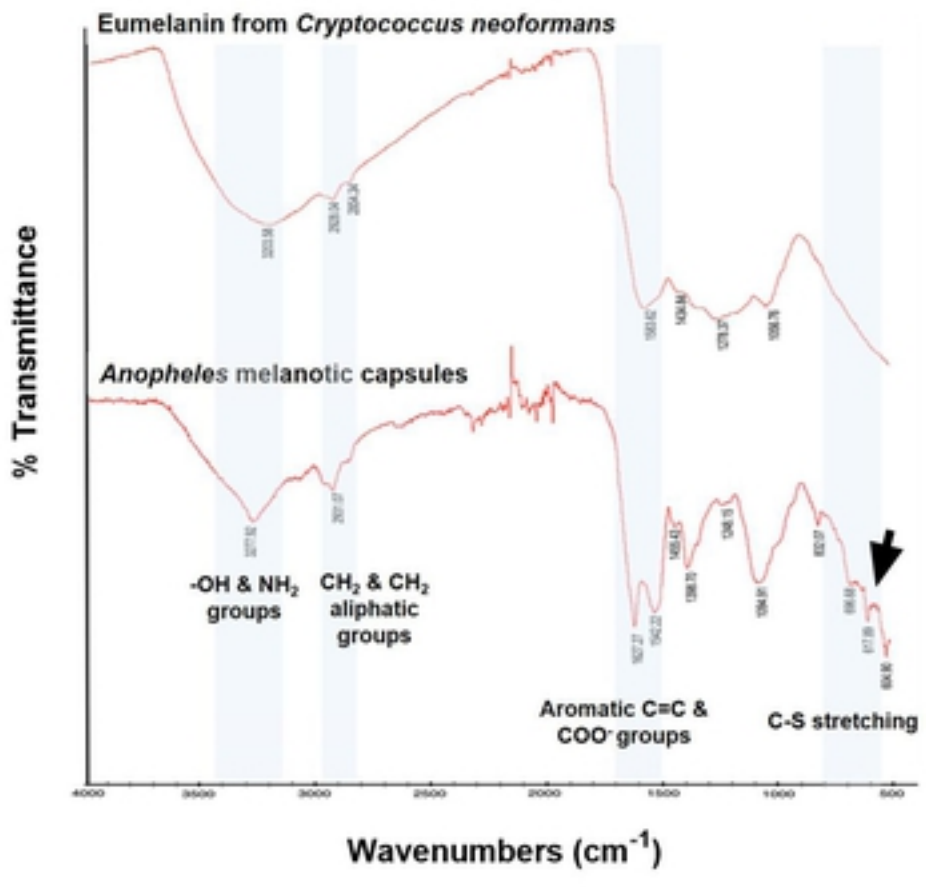

Figure1

bioRxiv preprint doi: https://doi.org/10.1101/2021.05.07.443077; this version posted May 8, 2021. The copyright holder for this preprint (which was not certified by peer review) is the author/funder, who has granted bioRxiv a license to display the preprint in perpetuity. It is made available under aCC-BY 4.0 International license.

A

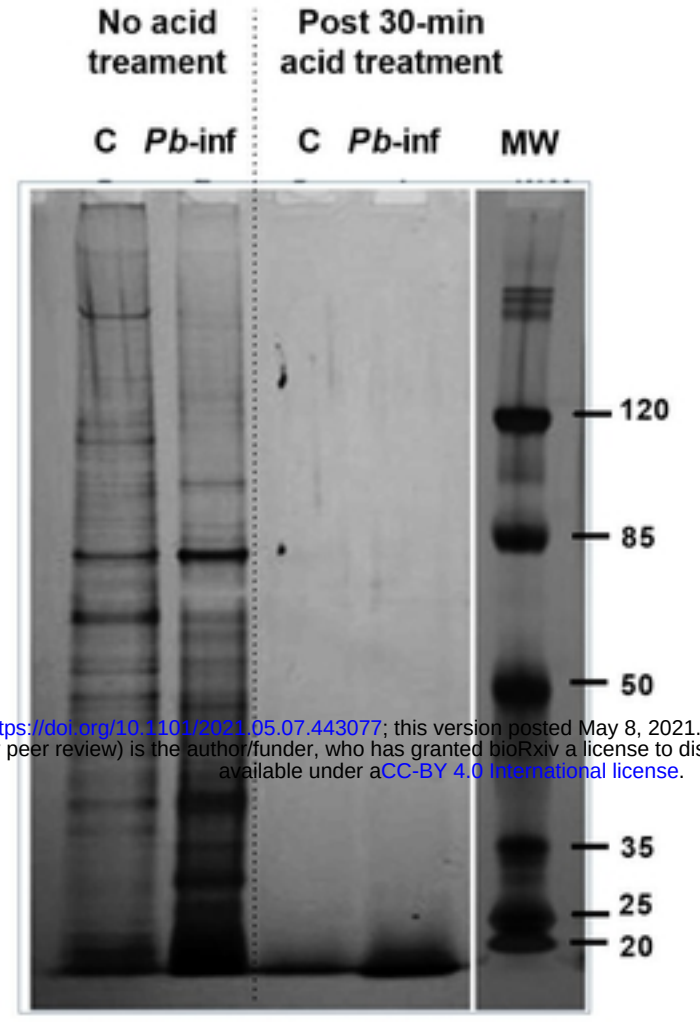

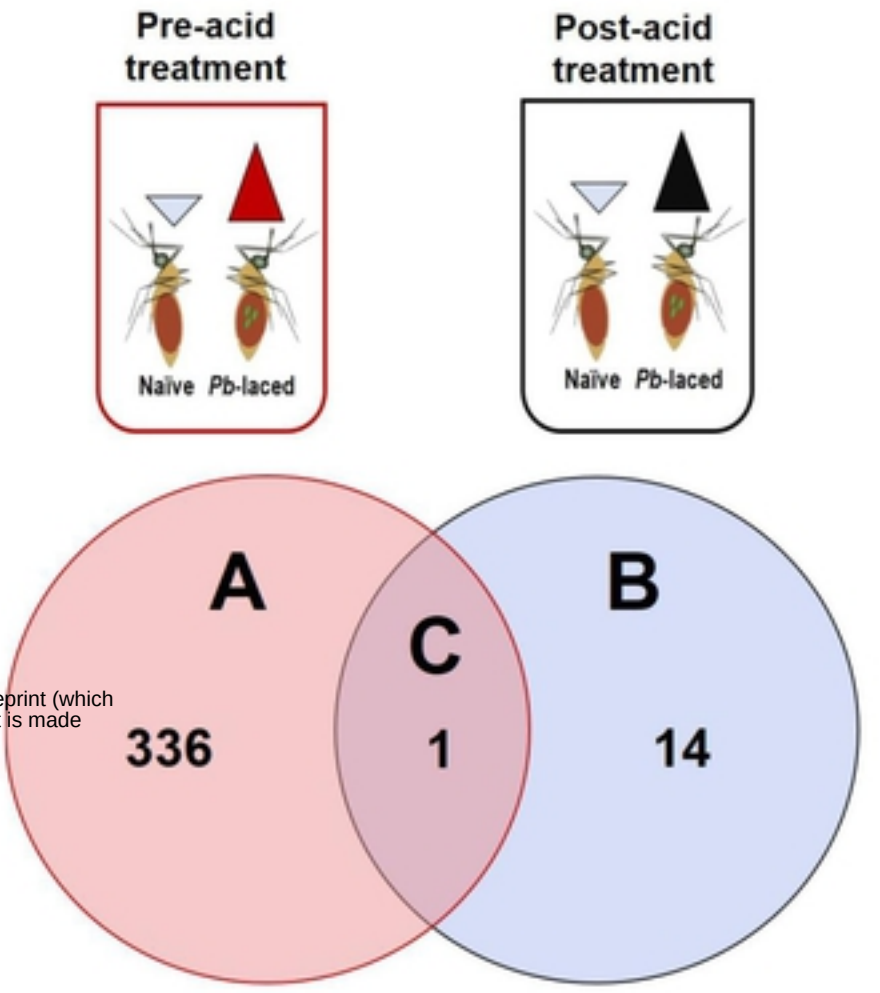

B

Accesion ID	Annotation	Pre-acid C	Pre-acid *Pb*-inf	Post-acid C	Post-acid *Pb*-inf	Cellular Localization
AGAP004742	Pyruvate carboxylase					Intracellular, Cytoplasm
AGAP000550	Uncharacterized protein					Extracellular Matrix
AGAP000881	Aldehyde dehydrogenase					Intracellular, Other
AGAP001151	14-3-3 protein epsilon					Intracellular, Cytoplasm
AGAP002884	V-type H+-transporting ATPase					Intracellular, Membrane
AGAP004877	Paramyosin					Intracellular, Cytoskeleton
AGAP005134	F-type H+-transporting ATPase					Intracellular, Membrane
AGAP007745	Peritrophic matrix-associated protein					Extracellular Matrix
AGAP007790	Sodium/potassium-transporting ATPase subunit beta					Intracellular, Membrane
AGAP009182	Protein transport SEC61					Intracelullar, Membrane
AGAP010147	Myosin heavy chain					Intracellular, Cytoskeleton
AGAP010479	Enolase binding protein (EBP)					Extracellular
AGAP012081	F1-ATPase					Intracellular, Other
AGAP012407	Protein disulfide-isomerase					Intracellular, ER

Figure2

A

	A. gambiae	*Ae. albopictus*	*Ae. aegypti*	*A. albimanus*	*A. dirus*	*A. stephensi*	*A. arabiensis*
A. gambiae		78.67%	78.33%	86.80%	88.43%	88.98%	99.72%
Ae. albopictus	78.67%		94.41%	76.95%	75.85%	74.57%	78.78%
Ae. aegypti	78.33%	94.41%		77.02%	75.58%	74.30%	78.37%
A. albimanus	86.80%	76.95%	77.02%		86.04%	83.02%	86.80%
A. dirus	88.43%	75.85%	75.58%	86.04%		84.95%	88.35%
A. stephensi	88.98%	74.57%	74.30%	83.02%	84.95%		89.18%
A. arabiensis	99.72%	78.78%	78.37%	86.80%	88.35%	89.18%	

B

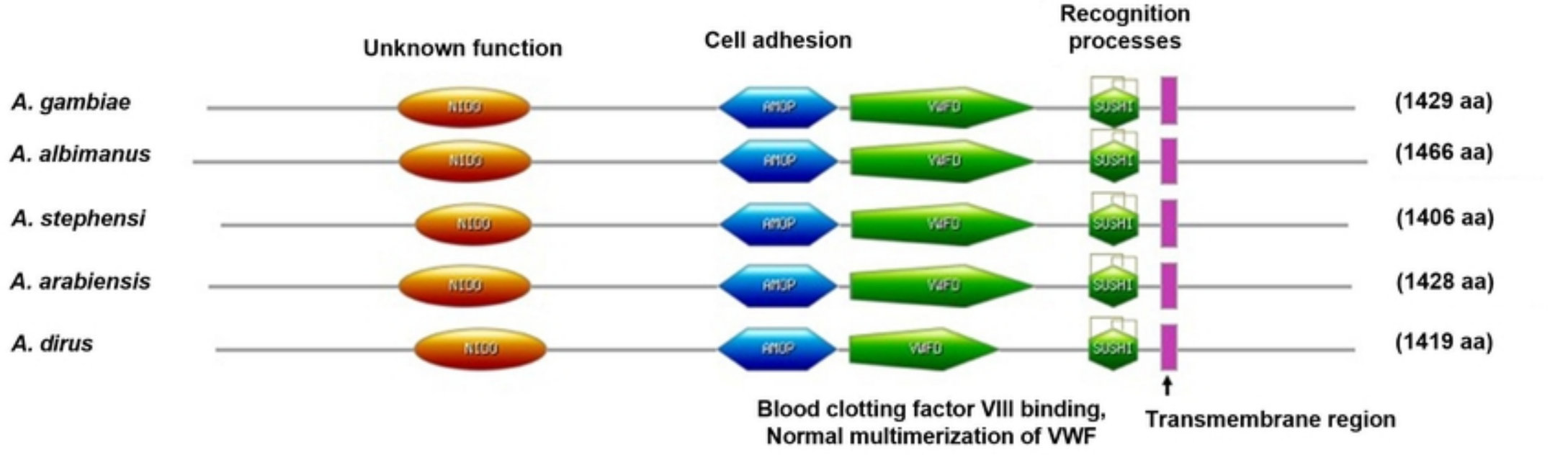

Figure3

bioRxiv preprint doi: https://doi.org/10.1101/2021.05.07.443077; this version posted May 8, 2021. The copyright holder for this preprint (which was not certified by peer review) is the author/funder, who has granted bioRxiv a license to display the preprint in perpetuity. It is made available under aCC-BY 4.0 International license.

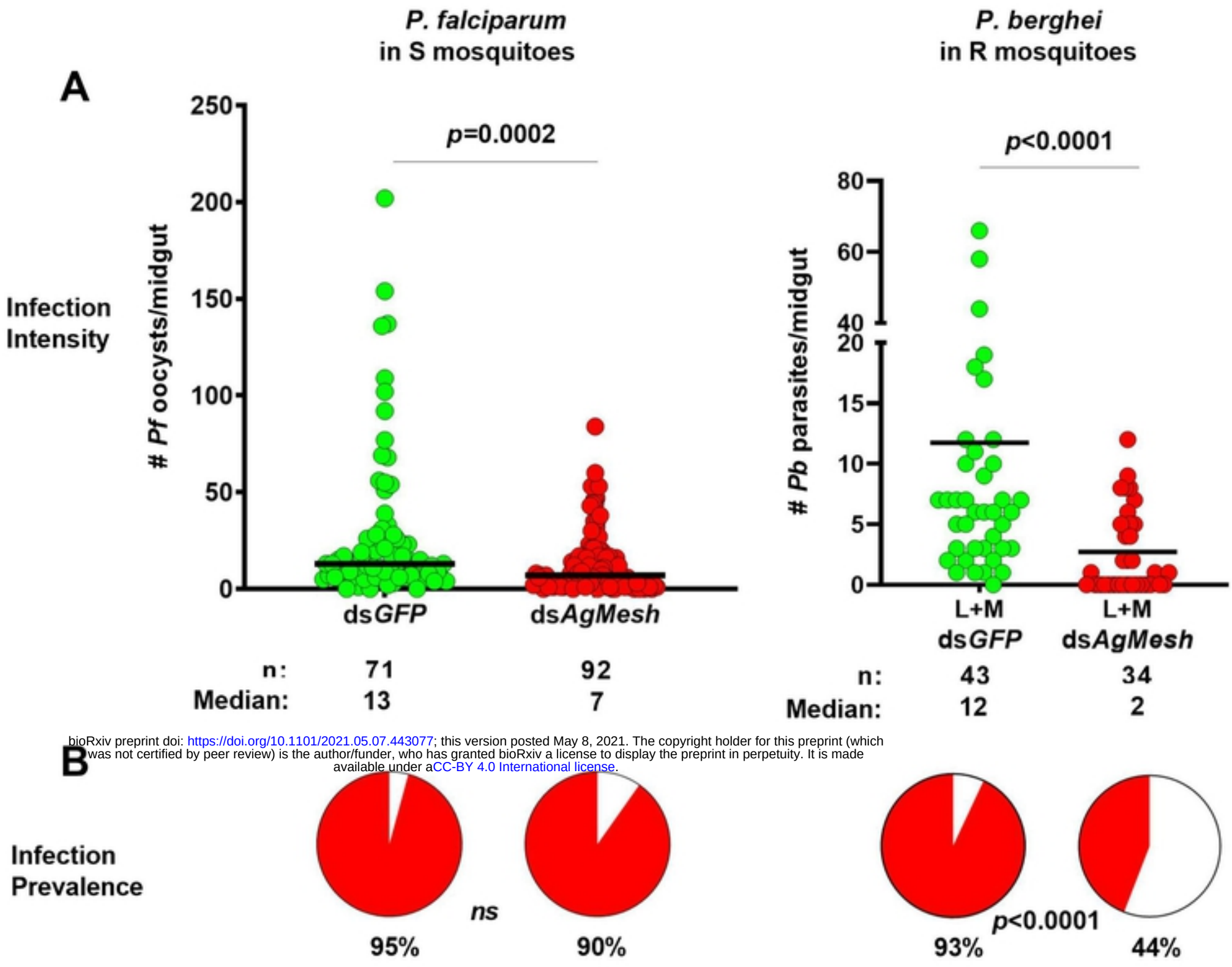

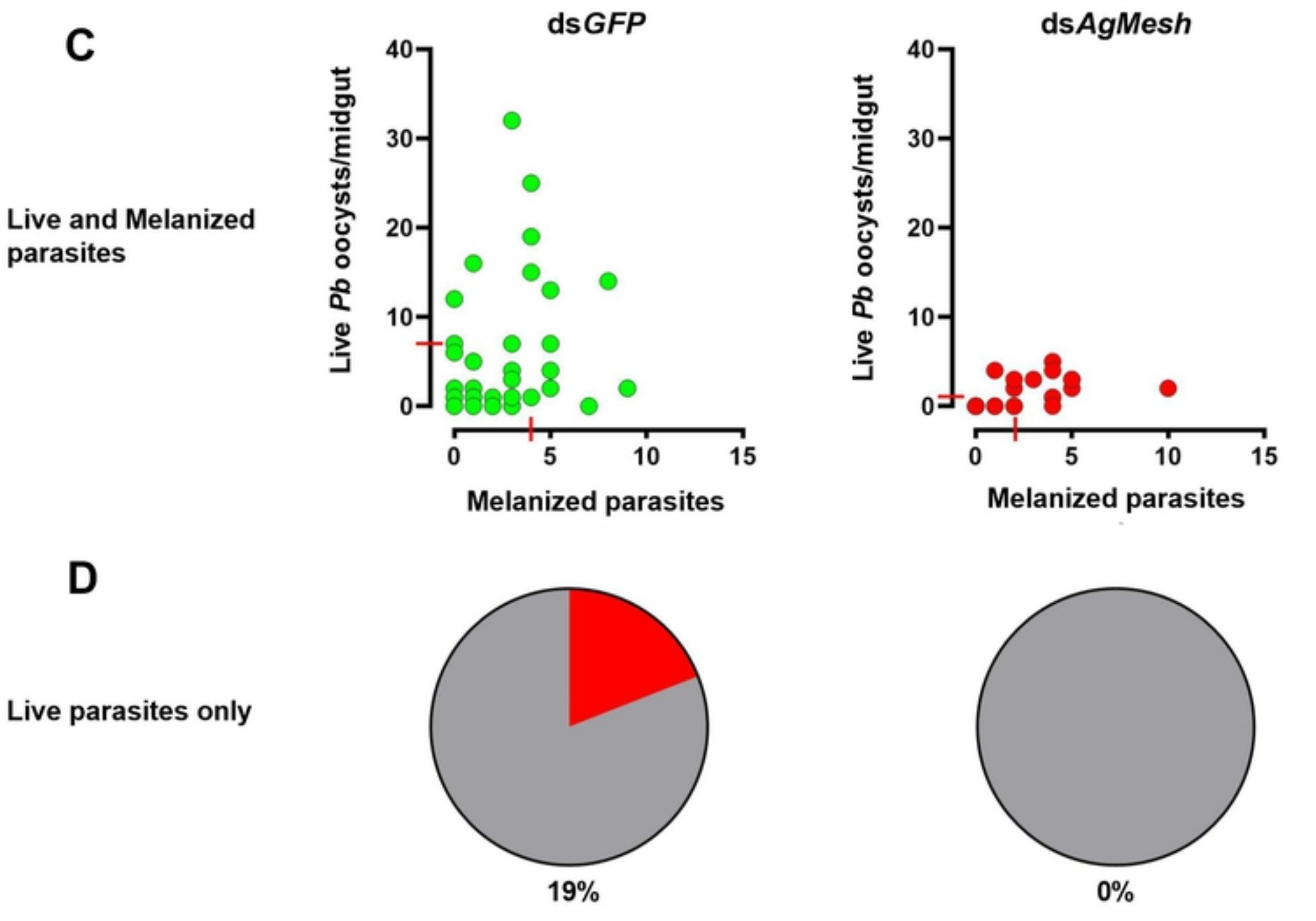

Figure4